Stem Cell Reports
Article
ISSCR
OPEN ACCESS

Inhibition of Apoptosis Reduces Diploidization of Haploid Mouse Embryonic Stem Cells during Differentiation

Wenhao Zhang,[1,4] Yaru Tian,[1,4] Qian Gao,[1,2,4] Xu Li,[1] Yanni Li,[3] Jinxin Zhang,[1] Chunmeng Yao,[1] Yuna Wang,[1] Haoyu Wang,[1] Yiding Zhao,[1] Qian Zhang,[1] Luyuan Li,[1] Yang Yu,[2,*] Yong Fan,[3,*] and Ling Shuai[1,*]

[1]State Key Laboratory of Medicinal Chemical Biology and College of Pharmacy, Nankai University, Tianjin 300350, China
[2]Reproductive Medical Center, Department of Gynecology and Obstetrics, Clinical Stem Cell Research Center, Peking University Third Hospital, Beijing 100191, China
[3]Key Laboratory for Major Obstetric Diseases of Guangdong Province, Key Laboratory of Reproduction and Genetics of Guangdong Higher Education Institutes, The Third Affiliated Hospital of Guangzhou Medical University, Guangzhou 510150, China
[4]Co-first author
*Correspondence: yuyang5012@hotmail.com (Y.Y.), yongfan011@gzhmu.edu.cn (Y.F.), lshuai@nankai.edu.cn (L.S.)
https://doi.org/10.1016/j.stemcr.2020.05.004

SUMMARY

Phenotypes of haploid embryonic stem cells (haESCs) are dominant for recessive traits in mice. However, one major obstacle to their use is self-diploidization in daily culture. Although haESCs maintain haploidy well by deleting *p53*, whether they can sustain haploidy in differentiated status and the mechanism behind it remain unknown. To address this, we induced *p53*-deficient haESCs into multiple differentiated lineages maintain haploid status *in vitro*. Haploid cells also remained in chimeric embryos and teratomas arising from *p53*-null haESCs. Transcriptome analysis revealed that apoptosis genes were downregulated in *p53*-null haESCs compared with that in wild-type haESCs. Finally, we knocked out *p73*, another apoptosis-related gene, and observed stabilization of haploidy in haESCs. These results indicated that the main mechanism of diploidization was apoptosis-related gene-triggered cell death in haploid cell cultures. Thus, we can derive haploid somatic cells by manipulating the apoptosis gene, facilitating genetic screens of lineage-specific development.

INTRODUCTION

Sexually reproductive diploid animals exhibit evolutionary advantages over asexual organisms due to meiosis and the combination of two haploid gametes from different genetic backgrounds (Kondrashov and Crow, 1991; Perrot et al., 1991). Diploid genomes have allelic backups, but this hinders the elucidation of the gene function of recessive traits. Recently developed haploid cell lines, including near-haploid tumor cells (Carette et al., 2009; Gibbons et al., 1991) and haploid embryonic stem cells (haESCs) (Leeb and Wutz, 2011; Sagi et al., 2016), greatly facilitate forward and reverse genetic screening in mammalian species (Li and Shuai, 2017). It is easy to identify not only toxicant-targeting genes (Elling et al., 2011) but also crucial genes regulating critical biological processes (such as differentiation [Leeb et al., 2014] or X chromosome inactivation [Monfort et al., 2015]) through high-throughput screening in haESCs. However, daily cultured haESCs tend to revert to diploid status, and periodic sorting for haploids is necessary, which hampers the application of these cell lines in genetic screening. In addition, haESCs undergo more severe diploidization during differentiation both *in vitro* and *in vivo*, making the derivation of haploid lineage-specific somatic cells very difficult (Shuai and Zhou, 2014). Therefore, spontaneous diploidization of haESCs jeopardizes the exploration of the application of haploid technology in mammalian organ development or disease-related genetic screening despite their original single-genome status.

Many efforts have been made to clarify the mechanism underlying the diploidization of mammalian haESCs; however, no precise regulatory pathway has yet been found. A previous report showed that the reason for the diploidization of mouse haESCs was a mistake in their cell cycle rather than the fusion of two single haploid cells, as indicated by the coculturing of haESCs with different marker genes (Leeb et al., 2012). Thereafter, chemical compounds inhibiting cell-cycle-related proteins were introduced into the culture medium to reduce diploidization (He et al., 2017; Takahashi et al., 2014), which still did not solve the problem completely. Single-cell dynamic analysis of mitosis in haESCs demonstrated that the metaphase of these cells was significantly longer than that of diploid ESCs (Guo et al., 2017). Thus, delayed mitosis might be the main cause of self-diploidization in haESCs. In this case, time-consuming and complicated fluorescence-activated cell sorting (FACS) was necessary to maintain the haploidy of haESCs. Recent studies showed that knockout of *p53* (Olbrich et al., 2017) or overexpression of *Dnmt3b* (He et al., 2018) could stabilize the haploid genome and slow down self-diploidization. In particular, *p53*-null haESCs could sustain haploid status well both under daily culture and in cells converting to an extraembryonic cell fate (Peng et al., 2019). *p53* is an essential gene related to the cell cycle, DNA damage, and other crucial biological

processes (Aladjem et al., 1998; Cross et al., 1995; Fujiwara et al., 2005). Nevertheless, whether the *p53*-null mutation is beneficial for the maintenance of a haploid status during differentiation is still unknown. The exact mechanism by which *p53*-null reduces self-diploidization is also not clear.

In this study, we deleted *p53* in mouse parthenogenetic haESCs with the CRISPR/Cas9 system and performed differentiation both *in vitro* and *in vivo* to assess whether *p53*-null stabilized haploidy in the somatic stage. The results revealed that by deleting *p53*, haploid somatic cells could be easily obtained from differentiated haESCs. We further analyzed global transcriptome data and found that genes regulating apoptosis were the main reason for diploidization during the differentiation of haESCs.

RESULTS

p53-Null HaESCs Maintain Haploidy Much More Stably Compared with Wild-Type HaESCs under Long-Term Culture

We generated two mouse parthenogenetic haESC lines from chemically activated oocytes according to a previous protocol (Shuai et al., 2014). These haESCs showed a standard mouse ESC morphology (Figure S1A) and grew well with the haploid genome assisted by FACS (Figure S1B). To introduce *p53* mutations in haESCs, we designed two Cas9-mediated *p53*-single guide RNA (sgRNA) vectors to perform electroporation (Figure S1C). Two days after transfection, approximately 58.6% of the analyzed cells were Cas9-GFP-positive (Figure S1D), and these cells were harvested for further culturing. We randomly picked three subclones from the sorted cultures and determined whether they were gene edited. All three subclones (*p53* KO-1, *p53* KO-2, and *p53* KO-3) carried different mutations in the *p53* gene according to DNA sequencing (Figure 1A). The T7EN1 cleavage assay results also confirmed this (Figure 1B). To assess whether the P53 protein was lost, we performed western blotting in *p53* KO-1, *p53* KO-2, *p53* KO-3, wild-type (WT) haESCs, and WT diploid ESCs (WT-diESCs). The results demonstrated that P53 was absent in all three *p53*-KO haESC lines (Figure 1C).

To determine whether *p53* mutation affects the pluripotency of haESCs, we examined specific markers and alkaline phosphatase activity in *p53*-KO haESCs. Positivity was observed not only for pluripotency markers (OCT4, NANOG, and SSEA-1) but also for alkaline phosphatase in *p53*-KO haESCs (Figures S1E and S1F). Karyotype analysis showed that most chromosome spreads of *p53*-KO haESCs contained 20 chromosomes (Figure S1G). Next, we analyzed pluripotent genes and *p53*-related genes in *p53*-KO haESCs by real-time PCR with WT-haESCs as a control. The expression levels of pluripotent markers (*Oct4* and *Nanog*) and *Cyclin B* did not change significantly in *p53*-KO haESCs compared with WT-haESCs. However, expression of *p53* and *p21* decreased, meanwhile *Cdk2* and *MAPK11* increased significantly in all three *p53*-KO haESC lines (Figure 1D). This result indicated that *p53* mutations did not affect pluripotency but do affect *p53*-related genes, including some cell-cycle genes. Since *p53* deletion increased haploidy maintenance in the ESC stage, as previously described, we tested whether *p53*-KO haESCs exhibited advantages in haploidy maintenance in daily culture without sorting for 3 weeks. There was still a high percentage of haploid cells remaining in the 1n peak (G_0/G_1 phase) of *p53*-KO haESCs (*p53* KO-1, 21.4%; *p53* KO-2, 20.9%; *p53* KO-3, 20.2%), whereas the percentage of the 1n peak (G_0/G_1 phase of haploid cells) in WT-haESCs decreased to 2.4% (Figure 1E). Here, we chose *p53* KO-1 (the most stable) for subsequent experiments. We designed *p53* overexpression (*p53* OE) vectors (Figure S1H) and transferred them into *p53* KO-1 cells having a high proportion of haploids, with an empty vector as control. After transfection, transfected cells expressing exogenous GFP (a GFP cassette was included in the *p53* OE vector or empty vector) were enriched for GFP and haploidy double-positive cells by FACS (Figures 1F and 1G). Real-time PCR result revealed that *p53* OE-haESCs (*p53* KO-1-*p53* OE) had re-expressed *p53* gene compared with WT-haESCs, *p53* KO-1, and *p53* KO-1-vector (Figure 1H). Western blotting analysis further confirmed this result (Figure S1I). Thereafter, we checked the haploidy-maintaining ability among *p53* KO-1, *p53* KO-1-vector, WT-haESCs, and *p53* KO-1-*p53* OE cells without sorting for 10 days (all the samples started as 100% of haploid cells). DNA-content analysis demonstrated that only *p53* KO-1 and *p53* KO-1-vector were able to maintain haploidy stably in this period, whereas *p53* KO-1-*p53* OE and WT-haESCs diploidized to some degree (Figure 1I). The rescue of *p53* expression in *p53*-KO haESCs made them unable to sustain the phenotype of stable haploidy any longer, which proved that *p53* was the main trigger of the diploidization phenomenon. As *Cdk2* and *MAPK11* (two important cell-cycle genes) were upregulated in *p53*-KO haESCs according to the above qPCR analysis, we conducted overexpression (OE) of *Cdk2* and *MAPK11* separately in WT-haESCs to address whether either of the two genes would affect the process of diploidization. Although the OE-haESCs showed upregulation of *Cdk2* and *MAPK11* independently (Figures S1J and S1K), neither of them obtained an advantage in maintaining haploidy like *p53*-KO in long-term cell culture (Figure S1L).

p53-Null HaESCs Differentiate Reliably with a Haploid Genome *In Vitro*

To examine the haploid-maintaining ability of *p53*-KO haESCs during differentiation *in vitro*, we performed

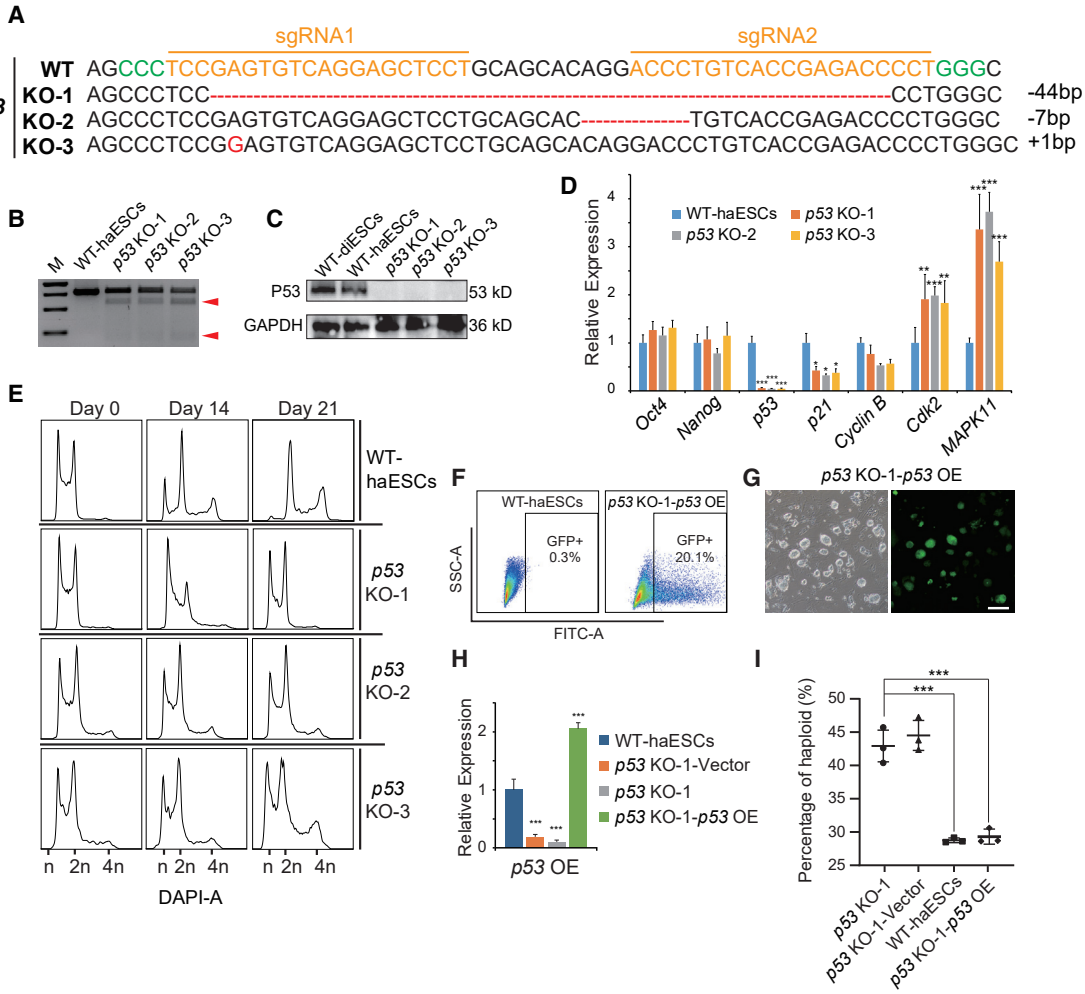

Figure 1. *p53* Deletion in haESC and DNA Analysis during Proliferation

(A). *p53*-deleted genotypes in subclones *p53* KO-1, *p53* KO-2, and *p53* KO-3.

(B) T7ENI cleavage analysis of the *p53*-KO lines *p53* KO-1, *p53* KO-2, and *p53* KO-3. Cleaved products (red arrowheads) indicate the presence of mutations.

(C) Western blotting to detect P53 in WT-diESCs, WT-haESCs, *p53* KO-1, *p53* KO-2, and *p53* KO-3 cells. GAPDH was used as a loading control.

(D) Expression levels of pluripotent, *p53*-related, and cell-cycle-related genes (*Oct4*, *Nanog*, *p53*, *p21*, *CyclinB*, *Cdk2*, and *MAPK11*) in WT-haESCs, *p53* KO-1, *p53* KO-2, and *p53* KO-3 cells determined by qPCR (n = 3 independent experiments). Data presented as mean ± SEM. t test: *p < 0.05, **p < 0.01, ***p < 0.001.

(E) DNA content analysis of *p53*-KO haESCs during culture on day 0, day 14, and day 21 without sorting, with WT-haESCs as a control. The percentages of the 1n (G_0/G_1) peak in WT-haESCs were 27.4%, 9.33%, and 2.4%, respectively; in *p53* KO-1 cells, 23.5%, 22.8%, and 21.4%, respectively; in *p53* KO-2 cells, 23.6%, 21.1%, and 20.9%, respectively; in *p53* KO-3 cells, 23.7%, 21.5%, and 20.2%, respectively.

(F) Percentage of GFP^+ cells in *p53* KO-1-*p53* OE cells after transfection. WT-haESCs without transfection were used as a negative control.

(G) Bright-field (BF) and FITC images of *p53* KO-1-*p53* OE cells, Scale bar, 100 μm.

(H) Expression levels of *p53* in WT-haESCs, *p53* KO-1-Vector, *p53* KO-1, and *p53* KO-1-*p53* OE cells determined by qPCR (n = 3 independent experiments). Data presented as mean ± SEM. t test: ***p < 0.001.

(I) Percentages of haploids in *p53* KO-1, *p53* KO-1-Vector, WT-haESCs, and *p53* KO-1-*p53* OE cells 10 days after sorting. Nearly 44% of sorted cells remained in haploidy in *p53* KO-1 and *p53* KO-1-Vector group, whereas WT-haESCs and *p53* KO-1-*p53* OE exhibited only 29% staying as haploid cells (n = 3 independent experiments). Data presented as mean ± SEM. t test: ***p < 0.001.

See also Figure S1 and Table S4.

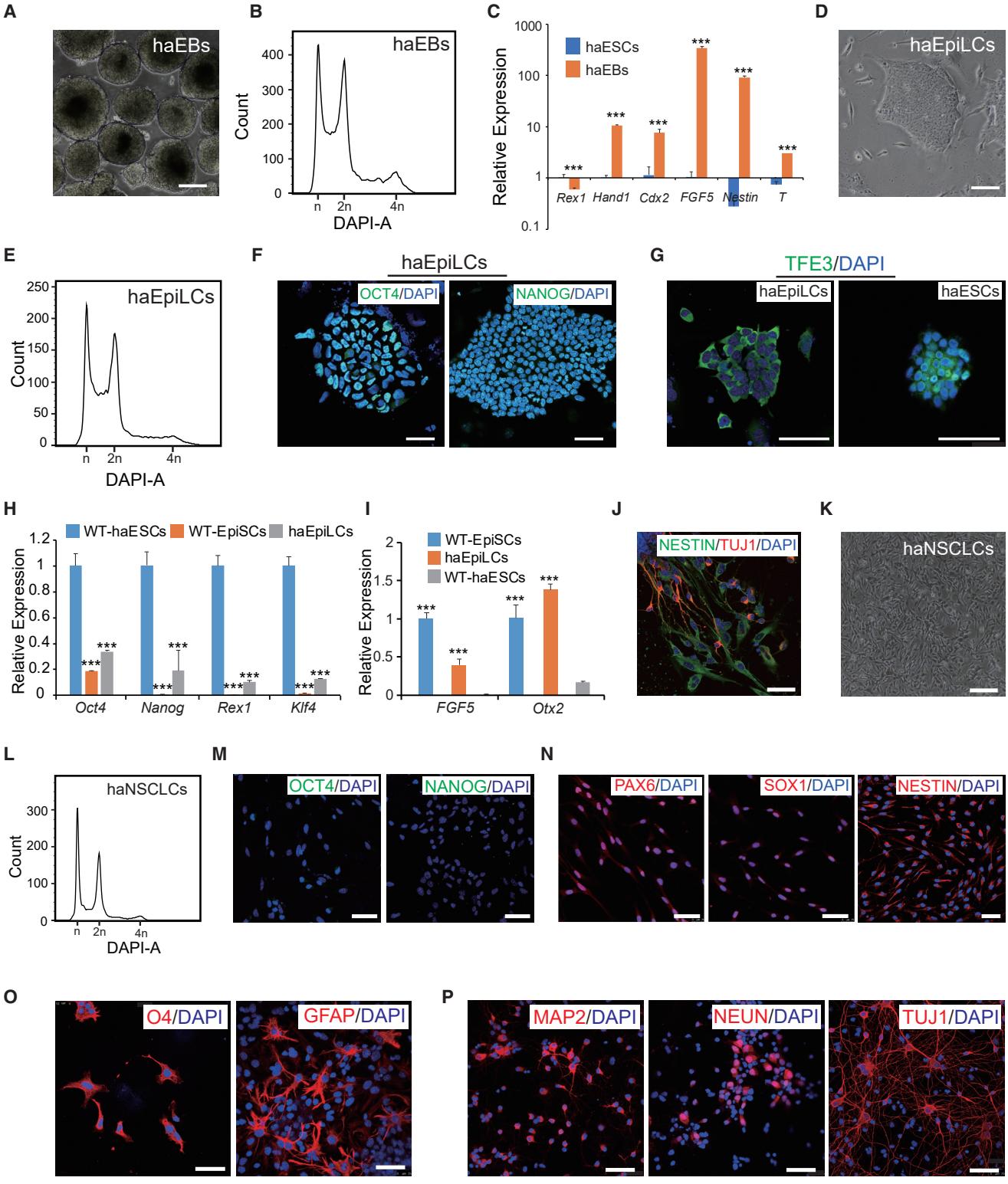

Figure 2. *In Vitro* Differentiation of *p53*-KO haESCs

(A) Morphology of 7-day haEBs derived from *p53* KO-1 cells. Scale bar, 100 μm.

(B) DNA-content analysis of 7-day haEBs derived from *p53* KO-1 cells. The percentage of the 1n (G_0/G_1) peak in haEBs was 21.7%.

(legend continued on next page)

differentiation of *p53*-KO haESCs at different stages. Standard embryoid bodies (EBs) formed (Figure 2A), and 29.7% of haploid cells (at G_0/G_1 phase) were observed in 7-day EBs from *p53*-KO haESCs (Figure 2B). The expression levels of pluripotency genes and specific genes of the three germ layers showed that the haploid EBs had differentiated beyond the ESC stage (Figure 2C). Although WT parthenogenetic haESCs were not able to remain in the epiblast stem cell-like cell (EpiLC) stage with a haploid genome (Leeb et al., 2012), *p53*-KO haESCs differentiated into haploid EpiLCs (haEpiLCs) quite easily and stably sustained haploidy (Figures 2D and 2E). The primed state haEpiLCs expressed pluripotent markers such as OCT4 and NANOG (Figure 2F). Besides, naive-primed distinguishing marker TFE3 (Betschinger et al., 2013) was located in the cytoplasm of haEpiLCs (Figure 2G), demonstrating that *p53*-KO haEpiLCs could remain in the epiblast stage with a single genome in the presence of basic fibroblast growth factor (bFGF) and activin A. The expression levels of specific genes further proved that these haploid cultures expressed primed stage genes (*FGF5* and O*tx2*), rather than naive genes (*Rex1* and *Klf4*), with WT-haESCs and WT epiblast stem cells (WT-EpiSCs) as controls (Figures 2H and 2I). To assess differentiation potentials of haEpiLCs, we induced neural differentiation according to a previous protocol (Ying et al., 2003). Around 7–10 days post differentiation, NESTIN- and TUJ1-positive cells were observed in the cell cultures (Figure 2J), indicating that haEpiLCs possessed pluripotency to differentiate to the next stage.

Although haploid neural progenitor cells (Elling et al., 2011) and haploid neurons (Xu et al., 2017) could be detected transiently, it is very difficult to obtain stable haploid neural stem cell-like cells (NSCLCs) by traditional methods. Whether *p53*-KO haESCs could differentiate into somatic stages and maintain haploidy required further investigation. We introduced endogenous NSCLC-specific *Pax6*-GFP into *p53*-KO haESCs according to our previous protocol (Li et al., 2018b). We performed neural differentiation of *p53* KO-1 cells and found that there were 22.3% of *Pax6*-GFP-positive cells among the differentiated derivatives (Figure S2A). Interestingly, there were 6.2% of *Pax6*-GFP-positive cells in the 1n peak, whereas there were 27.8% of *Pax6*-GFP-negative cells in the 1n peak (Figure S2B). These findings demonstrated that diploidization occurred but was slowed down during the differentiation of *p53*-KO haESCs. Haploid and *Pax6*-GFP double-positive cells were enriched by FACS to derive haNSCLCs for further culture. The haNSCLCs showed the standard neural stem cell morphology when cultured under adherent conditions (Figure 2K), presenting the ability to aggregate into neural spheres (Figure S2C). DNA analysis revealed that the haNSCLCs could stably maintain haploidy during proliferation (Figure 2L). Next, we examined pluripotent and neural stem cell-specific markers in haNSCLCs by immunostaining. Pluripotent markers (OCT4 and NANOG) were absent in haNSCLCs (Figure 2M). Positivity for PAX6, SOX1, and NESTIN was observed in adherent haNSCLCs (Figure 2N) and their neural spheres (Figure S2D). To assess the differentiation potential of haNSCLCs, we performed neural lineage specification. The results showed that glial cells (O4 and glial fibrillary acidic protein [GFAP] positive) and multiple neurons (MAP2, NEUN, and TUJ1 positive) could be generated from haNSCLCs (Figures 2O and 2P). In another parallel experiment, we analyzed DNA contents of glial mixture and neuronal mixture independently. There was 2.0% of glial mixture and 4.5% of neuronal

(C) Expression levels of pluripotency and differentiation genes (*Rex1*, *Hand1*, *Cdx2*, *Fgf5*, *Nestin*, and *T*) in haEBs and haESCs determined by qPCR (n = 3 independent experiments). Data presented as mean ± SEM. t test: ***p < 0.001.
(D) Morphology of haEpiLCs derived from *p53* KO-1 cells. Scale bar, 100 μm.
(E) DNA-content analysis of haEpiLCs derived from *p53* KO-1 cells. The percentage of the 1n (G_0/G_1) peak in haEpiLCs was 21.8%.
(F) Immunofluorescence of OCT4 and NANOG in haEpiLCs derived from *p53* KO-1 cells. DNA was stained with DAPI. Scale bar, 50 μm.
(G) Immunofluorescence of TFE3 in haEpiLCs derived from *p53* KO-1 cells and haESCs. DNA was stained with DAPI. Scale bar, 50 μm.
(H) Expression levels of pluripotency genes (*Oct4*, *Nanog*, *Rex1*, and *Klf4*) in WT-haESCs, WT-EpiSCs, and haEpiLCs determined by qPCR (n = 3 independent experiments). Data presented as mean ± SEM. t test: ***p < 0.001.
(I) Expression levels of EpiSC-specific marker genes (*Fgf5* and *Otx2*) in WT-haESCs, WT-EpiSCs and haEpiLCs determined by qPCR (n = 3 independent experiments). Data presented as mean ± SEM. t test: ***p < 0.001.
(J) Immunostaining of NESTIN and TUJ1 in 10-day differentiation cell cultures of haEpiLCs. Scale bar, 50 μm.
(K) Morphology of haNSCLCs derived from *p53* KO-1 cells. Scale bar, 100 μm.
(L) DNA-content analysis of haNSCLCs derived from *p53* KO-1 cells. The percentage of the 1n (G_0/G_1) peak in haNSCLCs was 28.5%.
(M) Immunofluorescence of OCT4 and NANOG in haNSCLCs. DNA was stained with DAPI. Scale bar, 50 μm.
(N) Immunofluorescence of neural stem cell-specific markers in haNSCLCs, PAX6, SOX1, and NESTIN. DNA was stained with DAPI. Scale bar, 50 μm.
(O) Immunostaining of oligodendrocytes (O4) and astrocytes (GFAP) derived from *p53* KO-1. Scale bar, 50 μm.
(P) Immunostaining of neuronal specific markers (MAP2, NEUN, and TUJ1) in neurons derived from *p53* KO-1. Scale bar, 50 μm.
See also Figure S2 and Table S4.

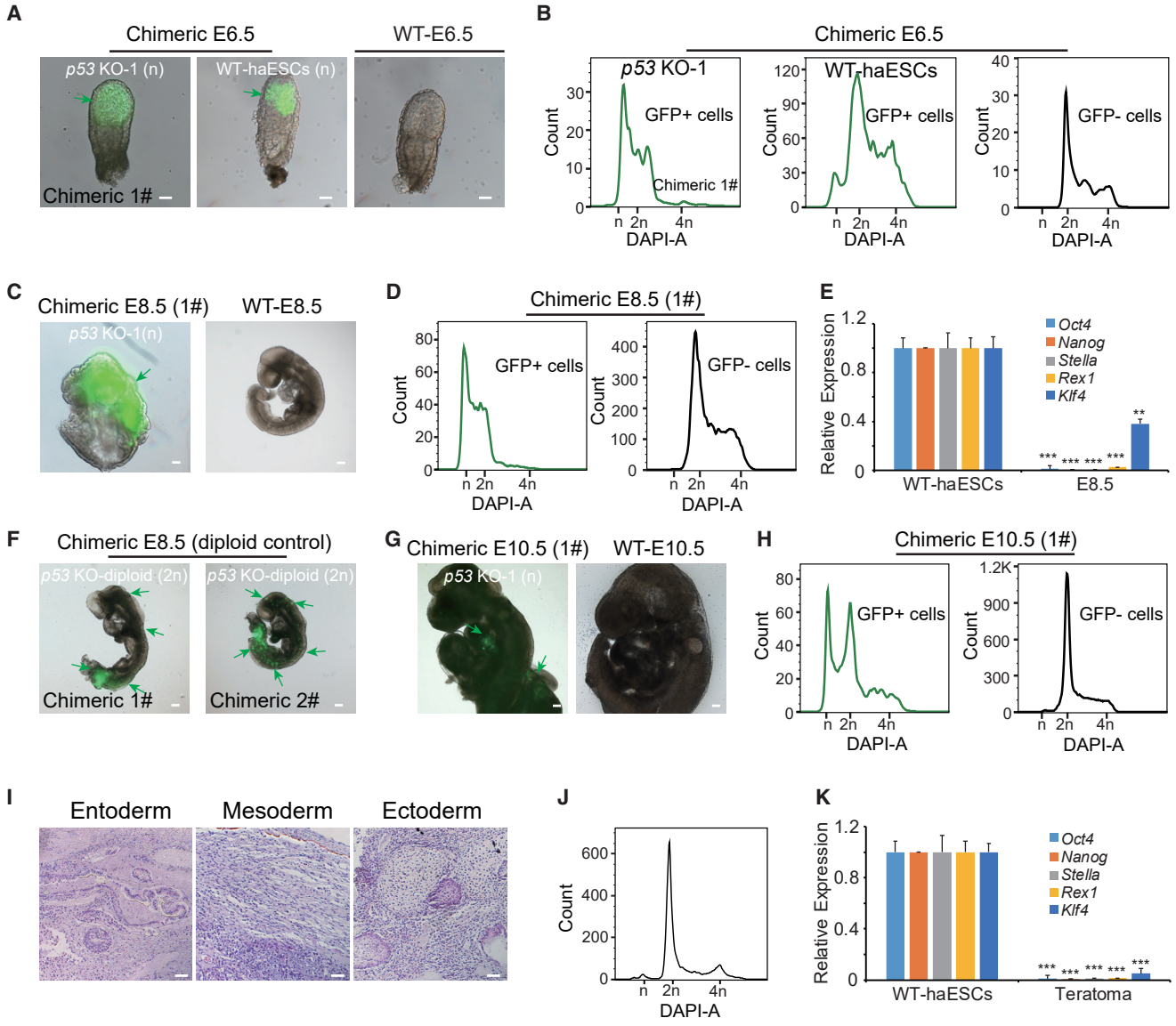

Figure 3. *In Vivo* Analysis of *p53*-KO haESCs

(A) Morphology of chimeric embryos at E6.5 derived from GFP-labeling WT-haESCs and *p53* KO-1 cells. Scale bar, 100 μm. WT-E6.5 embryo was used as a control.

(B) DNA-content analysis of GFP^+ cells and GFP^- cells in chimeric E6.5 embryos derived from GFP-labeling WT-haESCs and *p53* KO-1 cells. The percentages of the 1n (G_0/G_1) peak in GFP^+ cells from *p53* KO-1 E6.5 and WT-haESCs E6.5 were 28.5% and 4.7%, respectively.

(C) Morphology of chimeric embryo at E8.5 derived from GFP-labeling *p53* KO-1 cells. WT-E8.5 embryo was used as a control.

(D) DNA-content analysis of GFP^+ cells and GFP^- cells in chimeric E8.5 embryo derived from GFP-labeling *p53* KO-1 cells. The percentage of the 1n (G_0/G_1) peak from *p53* KO-1 chimeric E8.5 GFP^+ cells was 25.3%.

(E) Expression levels of pluripotency genes (*Oct4*, *Nanog*, *Stella*, *Rex1*, and *Klf4*) in chimeric E8.5 haploid cells from GFP^+ cells, with WT-haESCs as a loading control (n = 3 independent experiments). Data presented as mean ± SEM. t test: $^{**}p < 0.01$, $^{***}p < 0.001$.

(F) Morphology of chimeric embryos at E8.5 derived from GFP-labeling *p53* KO-diploid cells.

(G) Morphology of chimeric embryos at E10.5 derived from GFP-labeling *p53* KO-1 cells. WT E10.5 was used as a control.

(H) DNA-content analysis of GFP^+ cells and GFP^- cells in chimeric E10.5 embryo derived from GFP-labeling *p53* KO-1 cells. The percentage of the 1n (G_0/G_1) peak from *p53* KO-1 chimeric E10.5 GFP^+ cells was 21.4%.

(I) Teratoma formed from *p53* KO haESCs was identified by H&E staining. Scale bar, 100 μm. The tissues shown were gut epithelium (endoderm), muscle (mesoderm), and neural tissue (ectoderm).

(J) DNA-content analysis of teratoma. The percentage of the 1n (G_0/G_1) peak from all the tissue was 3.1%.

(legend continued on next page)

mixture remaining in the 1n peak, respectively (Figures S2E and S2F), indicating that haNSCLCs possessed multipotency for neural lineages with a haploid genome.

Haploid Cells Can Contribute to Chimeric Fetuses and Teratomas upon *p53* Knockout

The finding that *p53*-KO haESCs showed excellent haploidy maintenance during differentiation *in vitro* led to the further investigation of whether they presented the same advantages during differentiation *in vivo*. We microinjected GFP-labeling *p53*-KO haESCs into blastocysts to construct chimeric embryos. The reconstructed embryos were transferred to the oviducts of 0.5 days post coitum (dpc) pseudopregnant mice. Chimeric embryonic day 6.5 (E6.5) embryos from GFP-labeling *p53*-KO haESCs and GFP-labeling WT-haESCs were obtained (Figures 3A and S3A). Around 17.2% cells of chimeric E6.5 1# embryo and 55.5% cells of chimeric E6.5 2# embryo generated from *p53*-KO haESCs microinjection were GFP-positive cells (Table S1). The haploid cells in the 1n peak of *p53*-KO haESCs-chimeric E6.5 embryos (*p53* KO-1, chimeric 1#, 28.5%; *p53* KO-2, chimeric 2#, 24.5%) were much higher than that in WT-haESCs-chimeric E6.5 embryo (WT-haESCs-chimeric, 4.7%) (Figures 3B and S3B; Table S1), demonstrating that *p53*-KO haESCs could contribute to an epiblast stage with a high proportion of haploid status. For chimeric E8.5 embryos, 12.4% cells of 1# embryo and 37.6% cells of 2# embryo from *p53*-KO haESCs microinjection were GFP-positive cells (Table S1). However, chimeric E8.5 embryos from *p53*-KO haESCs were abnormal (Figures 3C and S3C), possibly due to the high contribution of haploid cells (a haploid genome might not support full development) or deficiency of *p53*, with approximately 25% of these cells (*p53* KO-1, chimeric 1#, 25.3%; *p53* KO-2, chimeric 2#, 24.3%) remaining in the 1n peak (Figures 3D and S3D). To address the identity of these haploid cells from E8.5 embryos, we harvested them by FACS and performed qPCR analysis. Compared with WT-haESCs, the sorted haploid cells barely expressed any of the pluripotent markers (*Oct4*, *Nanog*, *Stella*, *Rex1*, and *Klf4*), demonstrating that they were indeed differentiated cells (Figure 3E). Thus, *p53*-KO haESCs could differentiate into a somite stage without diploidization. To investigate the effect of *p53* deletion on development, we microinjected GFP-labeling *p53*-KO diploid ESCs into blastocysts as a parallel experiment. Interestingly, chimeric E8.5 embryos from *p53*-KO diploid ESCs were normal (Figure 3F), with GFP cells (24.9% in 1# and 40.3% in 2#) contributing to the chimeric E8.5 embryos (Table S1). Furthermore, abnormal chimeric E10.5 embryos were also able to be obtained (Figures 3G and S3E). The percentages of GFP cells in chimeric E10.5 1# and 2# embryos from *p53*-KO haESCs microinjection were 1.6% and 3.3%, respectively (Table S1). According to DNA analysis, there were still around 22% of haploid cells in 1n peak (*p53* KO-1, chimeric 1#, 21.4%; *p53* KO-2, chimeric 2#, 22.3%) from E10.5 GFP-positive cells (Figures 3H and S3F), indicating that *p53*-KO haESCs could further differentiate in a haploid genome with limited development potentials.

To check the pluripotency of *p53*-KO haESCs to form the three germ layers, we injected approximately 1×10^7 *p53* KO-1 cells under the skin of severe combined immunodeficiency (SCID) mice. Three weeks later, a standard teratoma formed (Figures S3G and S3H) and was divided into two parts. Histological analysis was performed on one part, and DNA-content analysis was performed on the other. Gut epithelium, muscle, and neural tube tissues, representing the three germ layers, were observed by H&E staining (Figure 3I). According to the DNA-content analysis, 3.1% haploid cells (1n peak) still existed in the 3-week teratoma, demonstrating that the *p53*-KO haESCs show a powerful ability to maintain haploidy *in vivo* (Figure 3J). The haploid cells from teratoma were also sorted by FACS and checked by qPCR. The result showed that the haploid cells in teratoma did not express the pluripotent marker genes (*Oct4*, *Nanog*, *Stella*, *Rex1*, and *Klf4*), indicating that they had entered a differentiated state instead of a pluripotent state (Figure 3K).

Transcriptome Analysis of *p53*-KO HaESCs

To determine why *p53*-KO haESCs show great advantages in haploidy maintenance, we compared the transcriptomes between *p53*-KO haESCs and WT-haESCs by RNA-sequencing (RNA-seq) analysis. The results revealed a very high correlation ($R^2 = 0.9947$) between *p53*-KO haESCs (*p53* KO-1, *p53* KO-2, and *p53* KO-3) and WT-haESCs (three independent WT-haESC lines) (Figure 4A). According to comprehensive summaries with all expression data (Tables S2 and S3), there were 2,785 differentially expressed genes ($p < 0.01$, fold change >2) between *p53*-KO haESCs and WT-haESCs, which were further analyzed to elucidate the reason of haploidy stabilization. Hierarchical clustering (heatmap) showed the top 50 differentially expressed genes between *p53*-KO haESCs and WT-haESCs, considering a fold change of 2.0 and $p < 0.05$ (Figure S4A and Table S2). These differentially expressed genes were mainly related to the extracellular matrix and basic development according to gene ontology (GO) analysis (Figures S4B and S4C).

(K) Expression levels of pluripotent genes (*Oct4*, *Nanog*, *Stella*, *Rex1*, and *Klf4*) in the 1n cells sorted from teratoma determined by qPCR, with WT-haESCs as a loading control (n = 3 independent experiments). Data presented as mean ± SEM. t test: ***$p < 0.001$.
See also Figure S2; Tables S1 and S4.

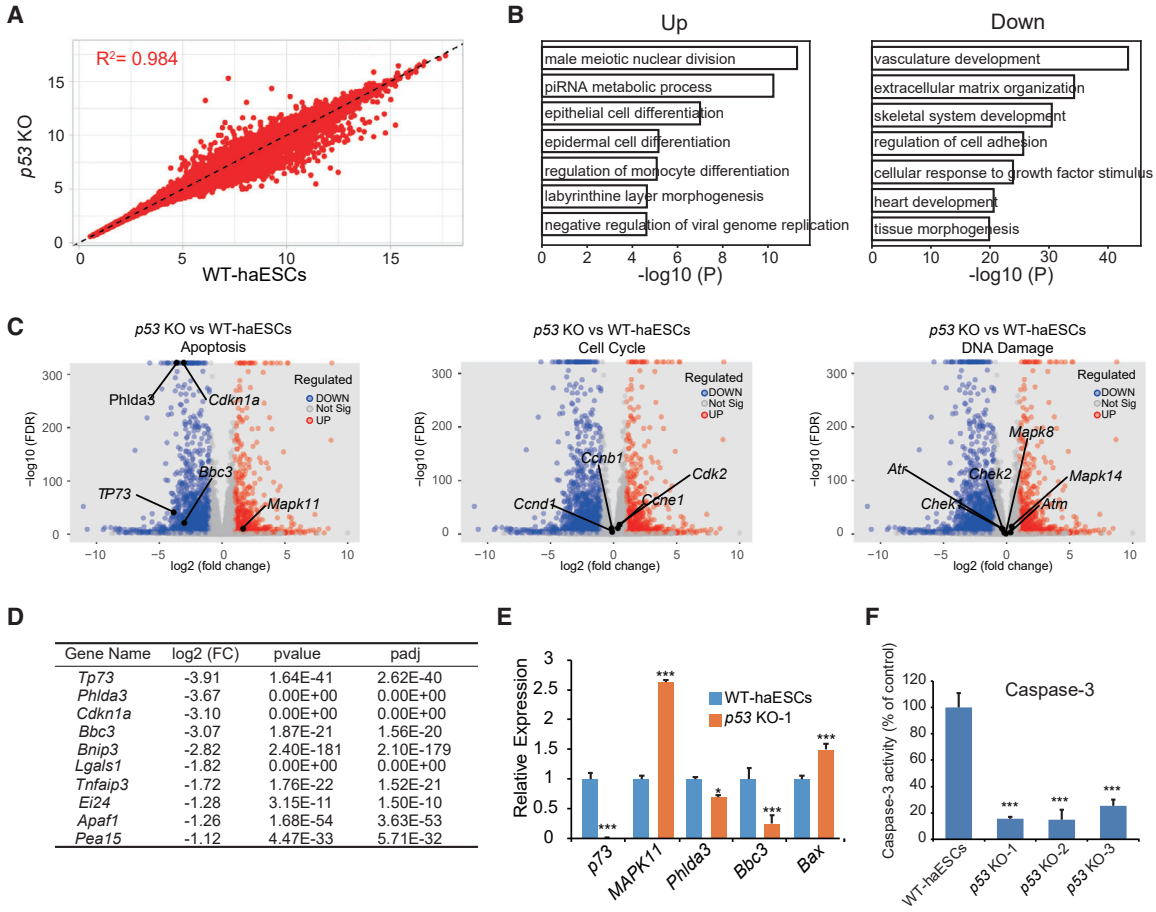

Gene Name	log2 (FC)	pvalue	padj
Tp73	-3.91	1.64E-41	2.62E-40
Phlda3	-3.67	0.00E+00	0.00E+00
Cdkn1a	-3.10	0.00E+00	0.00E+00
Bbc3	-3.07	1.87E-21	1.56E-20
Bnip3	-2.82	2.40E-181	2.10E-179
Lgals1	-1.82	0.00E+00	0.00E+00
Tnfaip3	-1.72	1.76E-22	1.52E-21
Ei24	-1.28	3.15E-11	1.50E-10
Apaf1	-1.26	1.68E-54	3.63E-53
Pea15	-1.12	4.47E-33	5.71E-32

Figure 4. Transcriptome of *p53*-KO haESCs

(A) Scatterplot of $\log_2$ transformed average gene expression profiles. Global gene expression of three *p53*-KO haESCs (*p53* KO-1, *p53* KO-2, and *p53* KO-3) and three WT-haESC lines (WT-haESCs-1, WT-haESCs-2, and WT-haESCs-3) were analyzed by scatterplot (R^2 is the Pearson correlation coefficient).

(B) Enriched gene ontologies of upregulated and downregulated genes in *p53*-KO haESCs.

(C) Volcano plot depicting the differential expression analysis between WT-haESCs and *p53*-KO haESCs. The higher location of the point of the gene, the more significant the difference. Highlighted points indicate genes correlated with apoptosis, cell cycle, and DNA damage, respectively, considering a fold change of 2.0 and $p < 0.05$.

(D) Top ten genes correlated with apoptosis in the differential expression analysis between WT-haESCs and *p53* KO haESCs.

(E) Expression levels of apoptosis-related genes (*p73*, *Phlda3*, *Bbc3*, and *Bax*) and a proliferation-related gene (*MAPK11*) in WT-haESCs and *p53*-KO haESCs determined by qPCR (n = 3 independent experiments). Data presented as mean ± SEM. t test: *$p < 0.05$, ***$p < 0.001$.

(F) Caspase-3 activity of *p53* KO-1, *p53* KO-2, and *p53* KO-3 cells, with WT-haESCs as a control (n = 3 independent experiments). Data presented as mean ± SEM. t test: ***$p < 0.001$.

See also Figure S4 and Tables S2, S3, and S4.

GO analysis data further indicated that most of the upregulated genes were correlated with male meiotic nuclear division, Piwi-interacting RNA metabolic process, and other biological processes, whereas the downregulated genes were related to vasculature development and extracellular matrix organization (Figure 4B). Since *p53* is a very important gene involved in multiple biological processes, including DNA-damage repair, cell-cycle arrest, and apoptosis (Hafner et al., 2019), we analyzed the expression of specific genes involved in these processes between *p53*-KO haESCs and WT-haESCs in volcano plots of p values ($-\log_{10}$ scale) versus fold changes ($\log_2$ scale). Interestingly, there were several differentially expressed genes related to apoptosis identified between the two groups (Figure 4C). However, we did not observe distinctly expressed genes related to the cell cycle or DNA damage in the RNA-seq data (Figure 4C). As we also found that the *p53*-KO haESCs showed better survival ability during differentiation

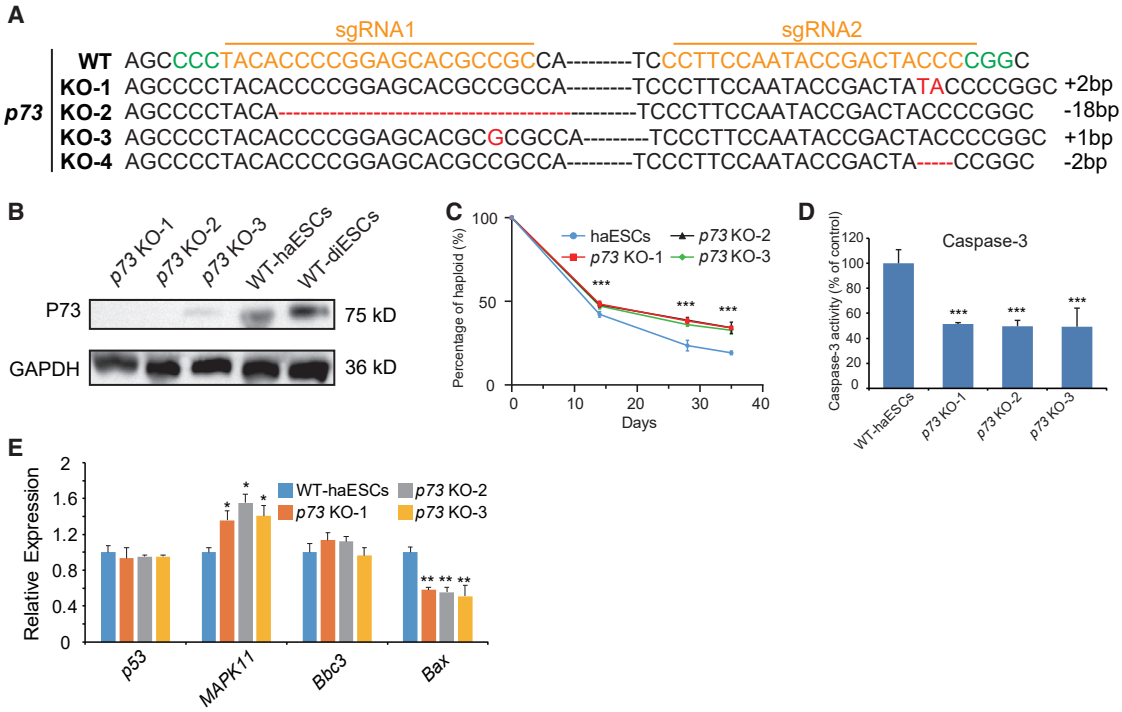

Figure 5. *p73* Is a Major Target of *p53*-Regulating Diploidization

(A) *p73*-deleted genotypes in haESCs by DNA sequencing.

(B) Western blot to detect P73 in *p73* KO-1 cells, *p73* KO-2 cells, *p73* KO-1 cells, WT-haESCs, and WT-diESCs. GAPDH was used as a loading control.

(C) Progression of the percentage of haploid cells in the *p73*-KO haESCs and WT-haESCs for 14 days, 28 days, and 35 days after sorting (n = 3 independent experiments). Data presented as mean ± SEM. t test: ***p < 0.001.

(D) Caspase-3 activity of *p73* KO-1, *p73* KO-2, and *p73* KO-3 cells, with WT-haESCs as a control (n = 3 independent experiments). Data presented as mean ± SEM. t test: ***p < 0.001.

(E) Expression levels of apoptosis-related genes (*p53*, *Bbc3*, and *Bax*) and proliferation-related gene *MAPK11* in *p73* KO-1, *p73* KO-2, and *p73* KO-3 haESCs determined by qPCR, with WT-haESCs as a control (n = 3 independent experiments). Data presented as mean ± SEM. t test: *p < 0.05, **p < 0.01.

See also Figure S5 and Table S4.

compared with WT-haESCs *in vitro* (data not shown), we assessed carefully the differentially expressed genes correlated with apoptosis. *TP73* (*p73*, also known as *Trp73*), *Phlda3*, *Cdkn1a*, and *Bbc3* (downstream target genes of *p53*) were significantly downregulated in *p53*-KO haESCs (Figure 4D) and were listed as the top four downregulated genes in *p53*-KO haESCs related to apoptosis. We further detected the expression levels of some target genes of *p53* related to apoptosis by qPCR and found that only *p73* and *Bbc3* were significantly downregulated (Figure 4E).

To address whether apoptosis was the main reason for the diploidization of haESCs, we assessed the survival rate of *p53*-KO haESCs 24 h after sorting for haploids compared with WT-haESCs. Nearly 70.5% of the sorted cells survived and expanded in the *p53*-KO group, whereas in the control group this percentage was only 52.9% (Figure S4D). As caspase-3 is a key molecule in the process of apoptosis (Song et al., 2015), we measured the caspase-3 activity between *p53*-KO haESCs and WT-haESCs after sorting. The caspase-3 activities in *p53* KO-1, *p53* KO-2, and *p53* KO-3 were significantly decreased compared with that in WT-haESCs (Figure 4F). In summary, apoptosis of *p53*-KO haESCs was reduced in daily culture and FACS processes.

p73 Is a Major Target of *p53*-Regulating Diploidization

To find out more about apoptosis-related gene-regulating diploidization, we designed *p73* and *Bbc3* knockout vectors (Figures S5A and S5B) and transfected them separately into WT-haESCs to introduce gene editing. Among the 60 randomly picked subclones of the *p73*-edited group, 25 subclones maintained haploidy (Figure S5C). We sequenced 11 subclones with high percentages of haploid cells and found that four of them were *p73*-KO cells

(Figure 5A). To assess whether the P73 protein was lost, we performed western blotting in *p73* KO-1, *p73* KO-2, *p73* KO-3, WT-haESCs, and diploid ESCs. The results demonstrated that P73 was absent in three *p73*-KO haESC lines (Figure 5B). However, in the *Bbc3*-edited group, 18 out of 60 randomly selected subclones exhibited haploid cells, 9 of which showed a high percentage of haploids, which were sequenced and did not contain a *Bbc3* mutation (Figure S5C). We randomly checked two diploidized subclones by sequencing and found *Bbc*3 mutations (Figure S5D). DNA-content analysis again confirmed that the *Bbc3* mutant subclones were diploid, without any haploid cells (Figure S5E). Notably, this result indicated that *p73* alone was the key regulator of diploidization, rather than *Bbc3*. We further assessed whether *p73*-KO haESCs also showed advantages in haploidy maintenance similar to those of *p53*-KO haESCs. The results demonstrated that *p73*-KO haESCs exhibited better proliferation ability after sorting (Figure S5F) and a lower rate of diploidization during long-term culture (Figure 5C) compared with WT-haESCs. The caspase-3 activity in *p73* KO-1, *p73* KO-2, and *p73* KO-3 was much lower than that in WT-haESCs, suggesting that apoptosis could be inhibited by *p73*-KO (Figure 5D). Next, we examined the expression of *p53*-targeted genes related to apoptosis in *p73*-KO haESCs (*p73* KO-1, *p73* KO-2 and *p73* KO-3) and WT-haESCs and did not find any significant differences in the downstream gene (Figure 5E). This result indicated that *p73* played a crucial role in affecting diploidization without interacting with its upstream genes, including *p53*.

DISCUSSION

Haploidy in lower organisms, including yeast, is fairly stable, which makes haploid individuals a powerful tool for genetic engineering (de Godoy et al., 2008). Medaka fish haESCs also show durable haploidy in both undifferentiated and differentiated statuses, despite being vertebrate species (Yi et al., 2009). However, mammalian haESCs tend to revert to diploidy under daily culture or differentiation, making complicated and frequent sorting of haploids necessary. Although haNSCLCs have been obtained by an optimized epiblast-based method (Shuai et al., 2015) or by introducing a ROCK inhibitor (Y27632) into the culture medium (He et al., 2017), these cells are not easy to handle, and the underlying mechanisms require further investigation. Our findings provide a simple strategy for deriving multiple haploid somatic cells by knocking out a single gene (*p53*-KO or *p73*-KO). We find that reduced apoptosis may be a major reason why *p53*-KO haESCs stably maintain haploidy. Additionally, knockout of *p73*, a target of *p53*, can also stabilize haploidy in haESCs.

Although *p53* or *p73* deficiency can promote haploidy maintenance in mouse haESCs, whether this phenomenon is applicable to other species remains unknown. Previous studies reported that primate haESCs maintain haploidy more stably than rodent haESCs (Sagi et al., 2016; Yang et al., 2013), and whether the mechanisms involved correlate with *p53* or *p73* warrants further investigation. Another study showed that although rhesus monkey haESCs maintained haploidy well in the ESC state, they underwent severe diploidization during differentiation for reasons related to apoptosis (Wang et al., 2018). Therefore, apoptosis may be the major cause of the diploidization of mammalian haploid cells. Generally, both haESCs and haploid somatic cells do not exhibit growth properties equivalent to those of their diploid counterparts (Olbrich et al., 2017). Our data revealed that *p53*-KO or *p73*-KO haESCs survived better after FACS (Figure S4D) and regained their proliferative ability faster (Figure S5F) than WT-haESCs. Previous studies have indicated that some haESCs experience cell-cycle errors such as mitosis escape, resulting in diploidization (Guo et al., 2017; He et al., 2017). According to our RNA-seq data, however, *p53*-KO haESCs did not show significant changes in the expression of cell-cycle-related genes (Figure 4C). We propose that the stabilization of haploidy in *p53*-KO haESCs depended on a reduction in apoptosis instead of regulation of the cell cycle. Nevertheless, both *p53* and *p73* are essential genes involved in many pathways, including key cell-cycle checkpoints (Melino et al., 2002; Stiewe, 2007). The exact mechanism by which *p53*-KO or *p73*-KO haESCs avoid mitosis escape has not yet been clarified.

Due to diploidization, complicated and time-consuming FACS purification is necessary for haploidy maintenance. Non-staining sorting methods have been introduced to enrich haploids (Freimann and Wutz, 2017; Qu et al., 2018), but their efficiency cannot be guaranteed. In our study, *p53*-KO or *p73*-KO haESCs could maintain haploidy without sorting for at least 3 weeks, which facilitates the expansion of large-scale haploid cell cultures rapidly for high-throughput genetic screening. However, previous reports demonstrated that *p53*-deficiency diploid ESCs showed limited pluripotency (Li et al., 2018a; Lin et al., 2005). In our study, *p53*-KO haESCs also showed nearly 2,800 differentially expressed genes from WT-haESCs at global transcriptome level. This indicated that there might be potential restriction of *p53*-KO haESCs in differentiation, which needs further investigation. Nevertheless, *p53*-KO haESCs could contribute to chimeras (up to E10.5) and teratomas in haploid status, which would mean that haploid somatic cells could be derived in a rigorous way *in vivo*, thus expanding the application of such a haploid system for lineage-specific genetic screening.

EXPERIMENTAL PROCEDURES

Transfection

To obtain *p53*-KO haESC lines, we electroporated approximately 4×10^6 WT-haESCs with PX461-sgRNA1 (3 μg) and PX461-sgRNA2 (3 μg), using a Neon (Invitrogen) electroporator at 1,400 V for 10 ms with three pulses. GFP-positive cells were sorted by FACS 2 days post electroporation. For the overexpression of *p53*, a combination of 2 μg of the *PBase* plasmid (SBI, PB210PA-1) and 6 μg of the overexpressing (or empty *piggyBac* control) plasmid were electroporated into 4×10^6 *p53*-KO haESCs using the same electroporating conditions described above. After transfection for 4–5 days, GFP and haploidy double-positive cells were sorted for subsequent experiments. Overexpression of *Cdk2* and *MAPK11* plasmids and *PBase* plasmid were transfected into WT-haESCs, respectively. After transfection for 4–5 days, GFP and haploidy double-positive cells were sorted for subsequent experiments. To obtain GFP-labeling cell lines, we electroporated a combination of 2 μg of the *PBase* plasmid (SBI, PB210PA-1) and 6 μg of the *piggyBac*-GFP plasmid into 4×10^6 *p53*-KO haESCs, *p53*-KO diESCs, or WT-haESCs, independently.

Differentiation of *p53*-KO haESCs

To detect the DNA contents of haploid embryonic bodies (haEBs) derived from *p53*-KO haESCs, we cultured the cells with Ndiff medium (Takara, Y40002) in noncoated Petri dishes (Falcon) for 7 days. EB aggregates were then dissociated with 0.05% trypsin/EDTA (Gibco, 25300062), and the DNA content was analyzed by FACS. To generate haEpiLCs, we added *p53* KO-1 cells to the wells of a 12-well plate coated with human fibronectin (Yeasen, 40105ES08) in EpiSC medium (Ndiff medium [Takara, Y40002] containing 20 ng/mL activin A [PeproTech, 120-14E-100] and 12 ng/mL bFGF [PeproTech, AF-100-18B-100]). The medium was changed every day, and standard EpiLC colonies emerged 2–3 days later. Fully grown haEpiLCs were passaged with 0.05% trypsin/EDTA and further cultured in EpiSC medium. After sorting for haploid cells 2–3 times (around 14 days), DNA content of haEpiSCs was analyzed. To generate haNSCLCs, we first established a *Pax6*-GFP *p53* KO-1 cell line as described previously (Li et al., 2018b). Four-day EB aggregates derived from *Pax6*-GFP *p53* KO-1 cells were then plated in fibronectin-precoated Petri dishes. After 9 days, *Pax6*-GFP-positive cells were sorted. The DNA content of the *Pax6*-GFP-positive/negative cells was then analyzed. Sorted *Pax6*-GFP-positive haploid cells were further cultured in N2B27 medium supplemented with 10 ng/mL EGF (PeproTech, AF-315-09-100) and 10 ng/mL bFGF (PeproTech, AF-100-18B-100) for proliferation.

For neuronal differentiation, haNSCLCs were plated into dishes precoated with poly-D-lysine (Sigma, P4957) and laminin (Sigma, L2020) and cultured in N2B27 medium supplemented with 20 ng/mL brain-derived neurotrophic factor (PeproTech, AF-450-02) and 20 ng/mL neurotrophin-3 (PeproTech, AF-450-03) to generate neurons. After 2 weeks, the differentiated haNSCLCs were examined for the expression of neuronal (TUJ1, MAP2, and NEUN) and oligodendroglial (O4) markers. For astrocyte differentiation, haNSCLCs were exposed to 1% fetal bovine serum and 10 ng/mL bone morphogenetic protein 4 (PeproTech, AF-120-05ET) in N2B27 medium for 5 days, followed by GFAP staining.

Chimeric Assay and Teratoma Formation

E6.5, E8.5, and E10.5 chimeric embryos were generated by injecting GFP-labeling *p53*-KO haESCs, *p53*-KO diploid ESCs, or WT-haESCs cells into CD-1 background blastocysts. Reconstructed embryos were transferred to the oviducts of pseudopregnant CD-1 mice at 0.5 dpc. At E6.5, E8.5, and E10.5, pseudopregnant mice were sacrificed to dissect chimeric fetuses. Chimeric embryos were trypsinized and GFP-positive and DNA-content analysis performed by FACS.

For teratoma analysis, approximately 1×10^7 *p53* KO-1 cells were injected subcutaneously into the limbs of 8-week-old male SCID mice. Fully formed teratomas were dissected 3 weeks later, then fixed in 4% paraformaldehyde, embedded in paraffin, sectioned, and stained with H&E for further analysis. Alternatively, fully formed teratomas were dissected to analyze the DNA contents.

Data and Code Availability

The Gene Expression Omnibus accession number for the RNA-seq data reported in this paper is GEO: GSE148118.

A complete description of the methods can be found in Supplemental Information.

SUPPLEMENTAL INFORMATION

Supplemental Information can be found online at https://doi.org/10.1016/j.stemcr.2020.05.004.

AUTHOR CONTRIBUTIONS

L.S. conceived and designed the study. W.Z., Y.T., and Q.G. performed most of the experiments. X.L., J.Z., C.Y., Y.W., H.W., Y.Z., and Q.Z. participated in some of the cell culture and molecular experiments. Y.L. analyzed the bioinformatics data. L.L., Y.Y., Y.F., and L.S. wrote the paper.

ACKNOWLEDGMENTS

This work was supported by the National Key Research and Development Program of China (2019YFA0109901 and 2018YFC1004101 to L.S., 2019YFA0110804 to Y.F.), "the Fundamental Research Funds for the Central Universities," Nankai University (63191731 to L.S.), the National Natural Science Foundation of China (31671538 and 31872841 to L.S., 81971381 and 81771580 to Y.Y.), and the Strategic Collaborative Research Program of the Ferring Institute of Reproductive Medicine, Ferring Pharmaceuticals, and Chinese Academy of Sciences (FIRMD181102 to L.S.).

Received: November 3, 2019
Revised: May 4, 2020
Accepted: May 4, 2020
Published: June 4, 2020

REFERENCES

Aladjem, M.I., Spike, B.T., Rodewald, L.W., Hope, T.J., Klemm, M., Jaenisch, R., and Wahl, G.M. (1998). ES cells do not activate p53-dependent stress responses and undergo p53-independent apoptosis in response to DNA damage. Curr. Biol. *8*, 145–155.

Betschinger, J., Nichols, J., Dietmann, S., Corrin, P.D., Paddison, P.J., and Smith, A. (2013). Exit from pluripotency is gated by intracellular redistribution of the bHLH transcription factor Tfe3. Cell *153*, 335–347.

Carette, J.E., Guimaraes, C.P., Varadarajan, M., Park, A.S., Wuethrich, I., Godarova, A., Kotecki, M., Cochran, B.H., Spooner, E., Ploegh, H.L., et al. (2009). Haploid genetic screens in human cells identify host factors used by pathogens. Science *326*, 1231–1235.

Cross, S.M., Sanchez, C.A., Morgan, C.A., Schimke, M.K., Ramel, S., Idzerda, R.L., Raskind, W.H., and Reid, B.J. (1995). A p53-dependent mouse spindle checkpoint. Science *267*, 1353–1356.

de Godoy, L.M., Olsen, J.V., Cox, J., Nielsen, M.L., Hubner, N.C., Frohlich, F., Walther, T.C., and Mann, M. (2008). Comprehensive mass-spectrometry-based proteome quantification of haploid versus diploid yeast. Nature *455*, 1251–1254.

Elling, U., Taubenschmid, J., Wirnsberger, G., O'Malley, R., Demers, S.P., Vanhaelen, Q., Shukalyuk, A.I., Schmauss, G., Schramek, D., Schnuetgen, F., et al. (2011). Forward and reverse genetics through derivation of haploid mouse embryonic stem cells. Cell Stem Cell *9*, 563–574.

Freimann, R., and Wutz, A. (2017). A fast and efficient size separation method for haploid embryonic stem cells. Biomicrofluidics *11*, 054117.

Fujiwara, T., Bandi, M., Nitta, M., Ivanova, E.V., Bronson, R.T., and Pellman, D. (2005). Cytokinesis failure generating tetraploids promotes tumorigenesis in p53-null cells. Nature *437*, 1043–1047.

Gibbons, B., MacCallum, P., Watts, E., Rohatiner, A.Z., Webb, D., Katz, F.E., Secker-Walker, L.M., Temperley, I.J., Harrison, C.J., Campbell, R.H., et al. (1991). Near haploid acute lymphoblastic leukemia: seven new cases and a review of the literature. Leukemia *5*, 738–743.

Guo, A., Huang, S., Yu, J., Wang, H., Li, H., Pei, G., and Shen, L. (2017). Single-cell dynamic analysis of mitosis in haploid embryonic stem cells shows the prolonged metaphase and its association with self-diploidization. Stem Cell Reports *8*, 1124–1134.

Hafner, A., Bulyk, M.L., Jambhekar, A., and Lahav, G. (2019). The multiple mechanisms that regulate p53 activity and cell fate. Nat. Rev. Mol. Cell Biol. *20*, 199–210.

He, Z.Q., Xia, B.L., Wang, Y.K., Li, J., Feng, G.H., Zhang, L.L., Li, Y.H., Wan, H.F., Li, T.D., Xu, K., et al. (2017). Generation of mouse haploid somatic cells by small molecules for genome-wide genetic screening. Cell Rep. *20*, 2227–2237.

He, W., Zhang, X., Zhang, Y., Zheng, W., Xiong, Z., Hu, X., Wang, M., Zhang, L., Zhao, K., Qiao, Z., et al. (2018). Reduced self-diploidization and improved survival of semi-cloned mice produced from androgenetic haploid embryonic stem cells through overexpression of Dnmt3b. Stem Cell Reports *10*, 477–493.

Kondrashov, A.S., and Crow, J.F. (1991). Haploidy or diploidy: which is better? Nature *351*, 314–315.

Leeb, M., and Wutz, A. (2011). Derivation of haploid embryonic stem cells from mouse embryos. Nature *479*, 131–134.

Leeb, M., Walker, R., Mansfield, B., Nichols, J., Smith, A., and Wutz, A. (2012). Germline potential of parthenogenetic haploid mouse embryonic stem cells. Development *139*, 3301–3305.

Leeb, M., Dietmann, S., Paramor, M., Niwa, H., and Smith, A. (2014). Genetic exploration of the exit from self-renewal using haploid embryonic stem cells. Cell Stem Cell *14*, 385–393.

Li, Y., and Shuai, L. (2017). A versatile genetic tool: haploid cells. Stem Cell Res. Ther. *8*, 197.

Li, M., Yu, J.S.L., Tilgner, K., Ong, S.H., Koike-Yusa, H., and Yusa, K. (2018a). Genome-wide CRISPR-KO screen uncovers mTORC1-mediated Gsk3 regulation in naive pluripotency maintenance and dissolution. Cell Rep. *24*, 489–502.

Li, Y., Li, X., Wang, H., Gao, Q., Zhang, J., Zhang, W., Zhang, Z., Li, L., Yu, Y., and Shuai, L. (2018b). CRISPR/Cas9-edited Pax6-GFP reporter system facilitates the generation of mouse neural progenitor cells during differentiation. J. Genet. Genomics *45*, 277–280.

Lin, T., Chao, C., Saito, S., Mazur, S.J., Murphy, M.E., Appella, E., and Xu, Y. (2005). p53 induces differentiation of mouse embryonic stem cells by suppressing Nanog expression. Nat. Cell Biol. *7*, 165–171.

Melino, G., De Laurenzi, V., and Vousden, K.H. (2002). p73: friend or foe in tumorigenesis. Nat. Rev. Cancer *2*, 605–615.

Monfort, A., Di Minin, G., Postlmayr, A., Freimann, R., Arieti, F., Thore, S., and Wutz, A. (2015). Identification of spen as a crucial factor for Xist function through forward genetic screening in haploid embryonic stem cells. Cell Rep. *12*, 554–561.

Olbrich, T., Mayor-Ruiz, C., Vega-Sendino, M., Gomez, C., Ortega, S., Ruiz, S., and Fernandez-Capetillo, O. (2017). A p53-dependent response limits the viability of mammalian haploid cells. Proc. Natl. Acad. Sci. U S A *114*, 9367–9372.

Peng, K., Li, X., Wu, C., Wang, Y., Yu, J., Zhang, J., Gao, Q., Zhang, W., Zhang, Q., Fan, Y., et al. (2019). Derivation of haploid trophoblast stem cells via conversion in vitro. iScience *11*, 508–518.

Perrot, V., Richerd, S., and Valero, M. (1991). Transition from haploidy to diploidy. Nature *351*, 315–317.

Qu, C., Yan, M., Yang, S., Wang, L., Yin, Q., Liu, Y., Chen, Y., and Li, J. (2018). Haploid embryonic stem cells can be enriched and maintained by simple filtration. J. Biol. Chem. *293*, 5230–5235.

Sagi, I., Chia, G., Golan-Lev, T., Peretz, M., Weissbein, U., Sui, L., Sauer, M.V., Yanuka, O., Egli, D., and Benvenisty, N. (2016). Derivation and differentiation of haploid human embryonic stem cells. Nature *532*, 107–111.

Shuai, L., and Zhou, Q. (2014). Haploid embryonic stem cells serve as a new tool for mammalian genetic study. Stem Cell Res. Ther. *5*, 20.

Shuai, L., Li, W., Wan, H., Zhao, X.Y., Wang, L., and Zhou, Q. (2014). Generation of Mammalian offspring by haploid embryonic stem cells microinjection. Curr. Protoc. Stem Cell Biol. *31*, 1A 6 1–15.

Shuai, L., Wang, Y., Dong, M., Wang, X., Sang, L., Wang, M., Wan, H., Luo, G., Gu, T., Yuan, Y., et al. (2015). Durable pluripotency and

haploidy in epiblast stem cells derived from haploid embryonic stem cells in vitro. J. Mol. Cell Biol. *7*, 326–337.

Song, J., Li, J., Hou, F., Wang, X., and Liu, B. (2015). Mangiferin inhibits endoplasmic reticulum stress-associated thioredoxin-interacting protein/NLRP3 inflammasome activation with regulation of AMPK in endothelial cells. Metab. Clin. Exp. *64*, 428–437.

Stiewe, T. (2007). The p53 family in differentiation and tumorigenesis. Nat. Rev. Cancer *7*, 165–168.

Takahashi, S., Lee, J., Kohda, T., Matsuzawa, A., Kawasumi, M., Kanai-Azuma, M., Kaneko-Ishino, T., and Ishino, F. (2014). Induction of the G2/M transition stabilizes haploid embryonic stem cells. Development *141*, 3842–3847.

Wang, H., Zhang, W., Yu, J., Wu, C., Gao, Q., Li, X., Li, Y., Zhang, J., Tian, Y., Tan, T., et al. (2018). Genetic screening and multipotency in rhesus monkey haploid neural progenitor cells. Development *145*, dev160531.

Xu, H., Yue, C., Zhang, T., Li, Y., Guo, A., Liao, J., Pei, G., Li, J., and Jing, N. (2017). Derivation of haploid neurons from mouse androgenetic haploid embryonic stem cells. Neurosci. Bull. *33*, 361–364.

Yang, H., Liu, Z., Ma, Y., Zhong, C., Yin, Q., Zhou, C., Shi, L., Cai, Y., Zhao, H., Wang, H., et al. (2013). Generation of haploid embryonic stem cells from *Macaca fascicularis* monkey parthenotes. Cell Res. *23*, 1187–1200.

Yi, M., Hong, N., and Hong, Y. (2009). Generation of medaka fish haploid embryonic stem cells. Science *326*, 430–433.

Ying, Q.L., Stavridis, M., Griffiths, D., Li, M., and Smith, A. (2003). Conversion of embryonic stem cells into neuroectodermal precursors in adherent monoculture. Nat. Biotechnol. *21*, 183–186.

Stem Cell Reports, Volume *15*

Supplemental Information

Inhibition of Apoptosis Reduces Diploidization of Haploid Mouse Embryonic Stem Cells during Differentiation

Wenhao Zhang, Yaru Tian, Qian Gao, Xu Li, Yanni Li, Jinxin Zhang, Chunmeng Yao, Yuna Wang, Haoyu Wang, Yiding Zhao, Qian Zhang, Luyuan Li, Yang Yu, Yong Fan, and Ling Shuai

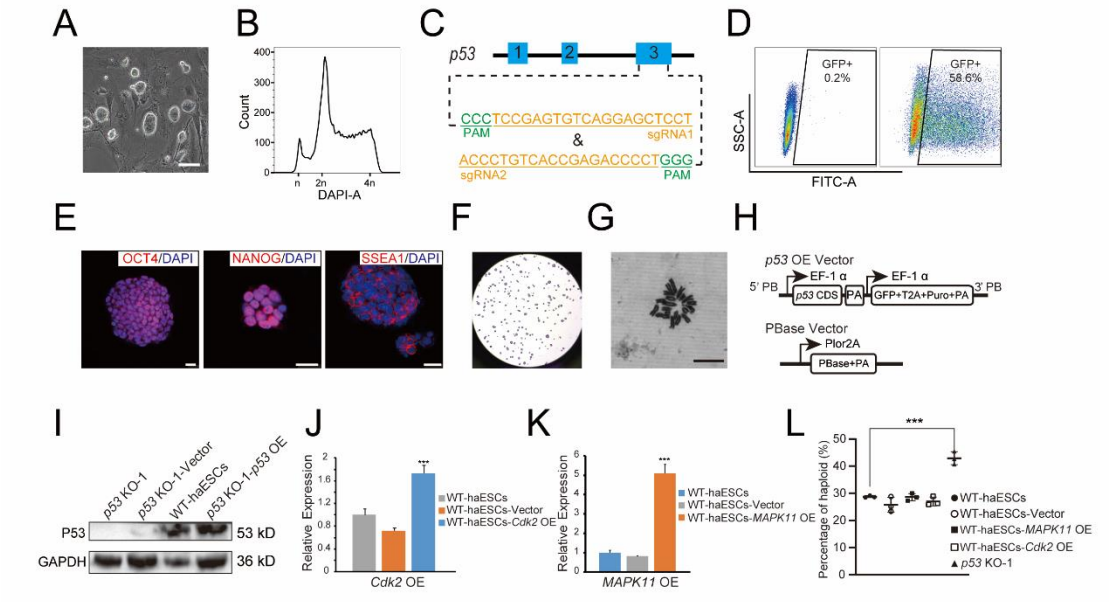

Figure S1. Gene editing in haESCs and characterization. Related to Figure 1

(A) Colonies of WT-haESCs in bright field. Scale bar, 100 μm.

(B) DNA content analysis of WT-haESCs for *p53*-deletion. The percentage of the 1n peak (G0/G1 phase) in WT-haESCs was 7.0%.

(C) DNA information for *p53* knocking out using the CRISPR/Cas9 system.

(D) Percentage of Cas9-GFP positive cells in transfected WT-haESCs 2 days after transfection by FACS indicating. WT-haESCs without transfection were used as control.

(E) Immunofluorescence staining of pluripotent markers, including OCT4, NANOG and SSEA1 in *p53*-KO haESCs. DNA was stained with DAPI. Scale bar, 50 μm.

(F) Alkaline phosphatase (AP) staining of *p53*-KO haESCs.

(G) Chromosome spread analysis of *p53*-KO haESCs. Scale bar, 10 μm.

(H) Schematic overview of the vectors used for overexpression of *p53*.

(I) Western blotting analysis of P53 in *p53* KO-1, *p53* KO-1-Vector, WT-haESCs and *p53* KO-1-*p53* OE cells. GAPDH was used as a loading control.

(J) Expression levels of *Cdk2* in WT-haESCs, WT-haESCs-Vector and WT-haESCs-*Cdk2* OE cells determined by qPCR. (n=3 independent experiments). t test, ***p < 0.001. Data was represented as the mean ± SEM.

(K) Expression levels of *MAPK11* in WT-haESCs, WT-haESCs-Vector and WT-haESCs-*MAPK11* OE cells determined by qPCR. (n=3 independent experiments). t test, ***p < 0.001. Data was represented as the mean ± SEM.

(L) Percentage of haploid cells in WT-haESCs, WT-haESCs-Vector, WT-haESCs-*MAPK11*-OE, WT-haESCs-*Cdk2*-OE and *p53*-KO haESCs at day 10 after sorting. Nearly 29% of sorted cells remained in haploidy in WT-haESCs-*Cdk2*-OE, WT-haESCs-*MAPK11*-OE, WT-haESCs and WT-haESCs-Vector, whereas *p53* KO-1 still had 44% of cells stayed in haploidy. (n=3 independent experiments). t test, ***p < 0.001. Data was represented as the mean ± SEM.

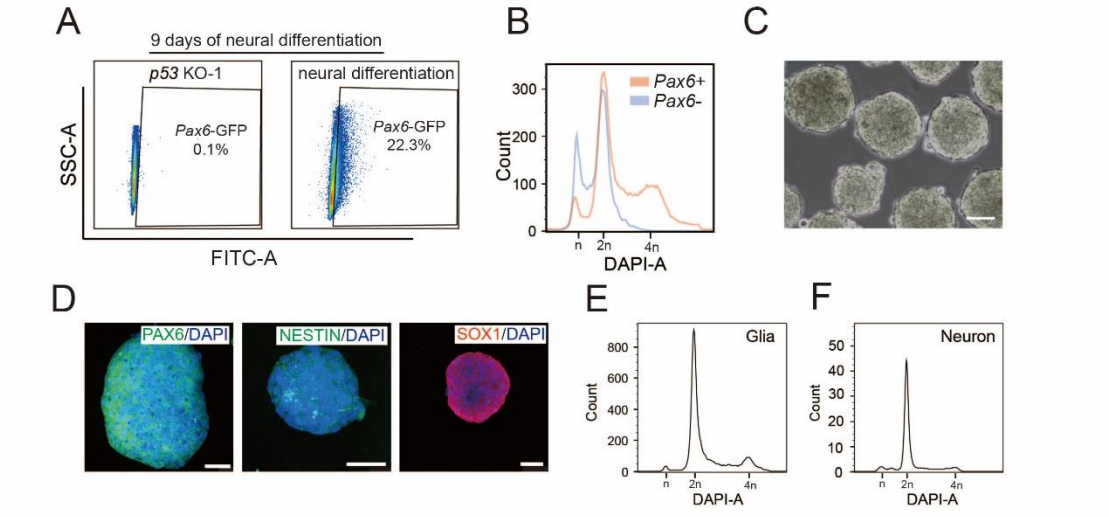

Figure S2. *In vitro* differentiation potentials of *p53*-KO haESCs. Related to Figure 2

(A) FACS analysis of *Pax6*-GFP-positive cells on 9-day of neural differentiation. *p53*-KO haESCs was used as the *Pax6*-GFP-negative control.

(B) DNA content analysis of *Pax6*-GFP-positive and -negative cells derived from *p53*-KO haESCs. The percentage of the 1n (G0/G1) peak in *Pax6*-GFP-positive cells was 6.2%, and that in *Pax6*-GFP-negative cells was 27.8%.

(C) The haNSCLCs spontaneously aggregate to form compact neural sphere structures in suspension culture. Scale bar, 100 μm.

(D) Immunostaining of PAX6, NESTIN and SOX1 in the neural spheres derived from *p53*-KO haESCs. Scale bar, 50 μm.

(E) DNA content analysis of glial mixture differentiated from haNSCLCs. 2.0% of cells remained in the 1n peak.

(F) DNA content analysis of neuronal mixture differentiated from haNSCLCs. 4.5% of cells remained in the 1n peak.

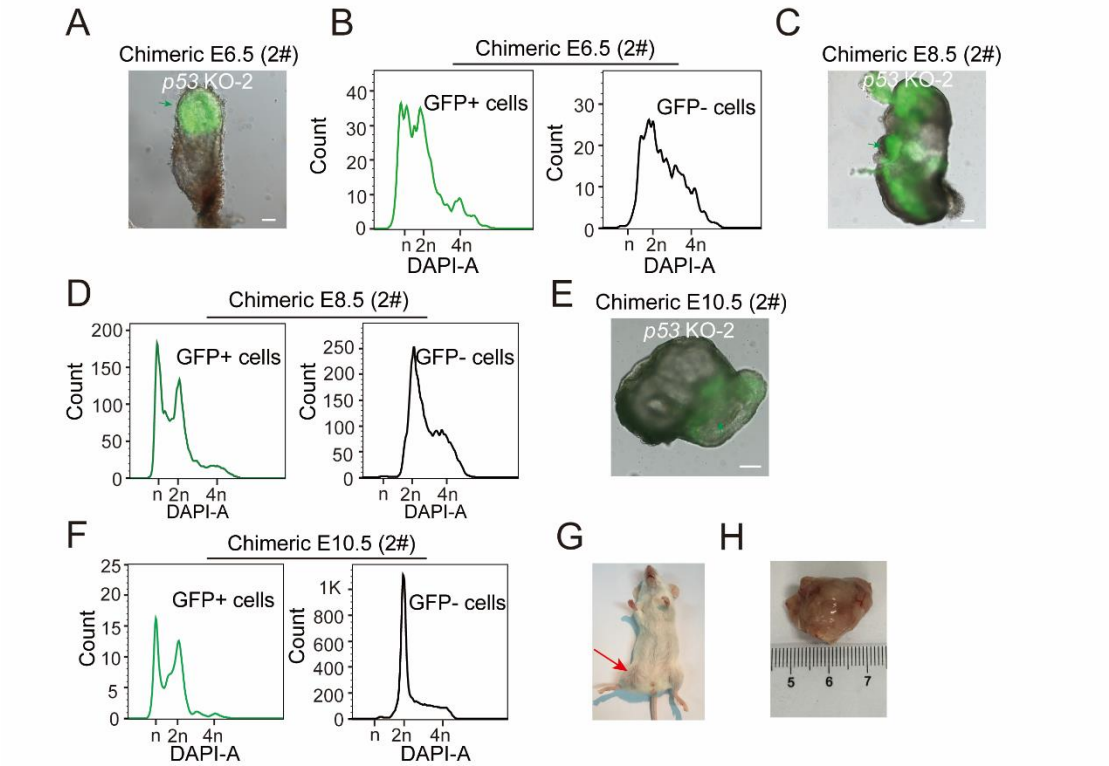

Figure S3. *In vivo* differentiation potentials of *p53*-KO haESCs. Related to Figure 3

(A) Morphology of chimeric embryo at E6.5 derived from GFP labelling *p53* KO-2 cells. Scale bar, 100 μm.

(B) DNA content analysis of GFP+ cells and GFP- cells in chimeric E6.5 embryo derived from *p53* KO-2 cells. The percentage of the 1n (G0/G1) peak in GFP+ cells was 24.5%.

(C) Morphology of chimeric embryo at E8.5 derived from GFP labelling *p53* KO-2 cells. Scale bar, 100 μm.

(D) DNA content analysis of GFP+ cells and GFP- cells in chimeric E8.5 embryo derived from *p53* KO-2 cells. The percentage of the 1n (G0/G1) peak in GFP+ cells was 24.3%.

(E) Morphology of chimeric embryo at E10.5 derived from GFP labelling *p53* KO-2 cells. Scale bar, 100 μm.

(F) DNA content analysis of GFP+ cells and GFP- cells in chimeric E10.5 with *p53* KO-2 cells. The percentage of the 1n (G0/G1) peak in chimeric GFP+ cells was 22.3%.

(G-H) Teratoma derived from *p53*-KO haESCs.

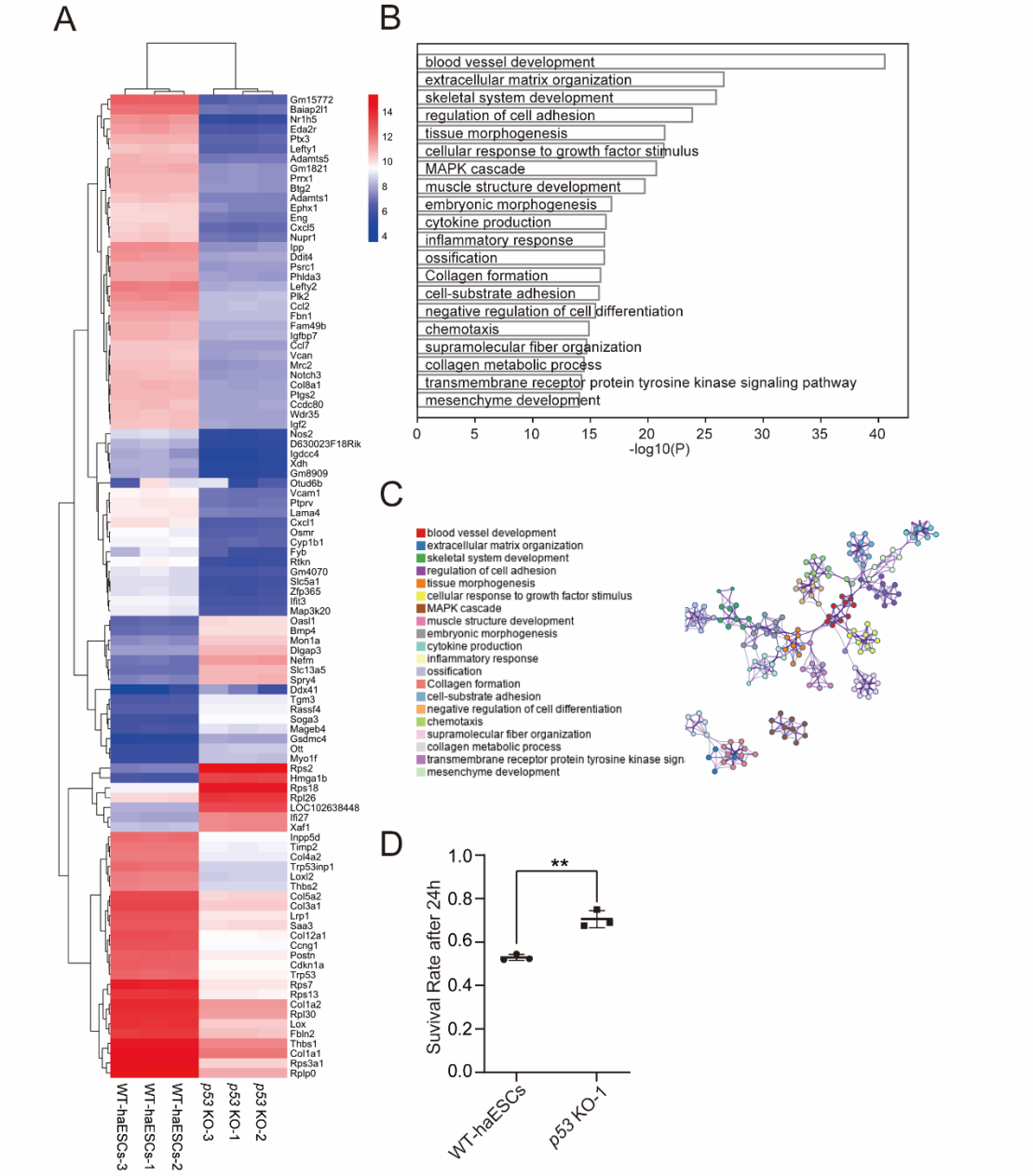

Figure S4. RNA-seq and survival analysis of *p53*-KO haESCs. Related to Figure 4

(A) Hierarchical clustering (heat map) showed the top 100 differentially expressed genes among WT-ESCs and *p53*-KO haESCs, considering a fold change of 2.0 and $p < 0.05$. To observe the differences between samples, we selected the top 50 variant genes.

(B) Enriched terms of differentially expressed genes in *p53*-KO haESCs (more than 2 folds) compared to WT-haESCs, statistical significance was represented by a discrete color scale.

(C) Enrichment network visualization for differential expressed genes between WT-haESCs and *p53*-KO haESCs. Each node represents an enriched term and cluster annotations are shown in color.

(D) Cell survival rates of WT-haESCs and *p53*-KO haESCs for 24 h after sorting. Nearly 70.5% of sorted cells survived in *p53*-KO haESCs, whereas that in WT-haESCs exhibited only 52.9%. (n=3 independent experiments). t test, $**p < 0.01$. Data was represented as the mean ± SEM.

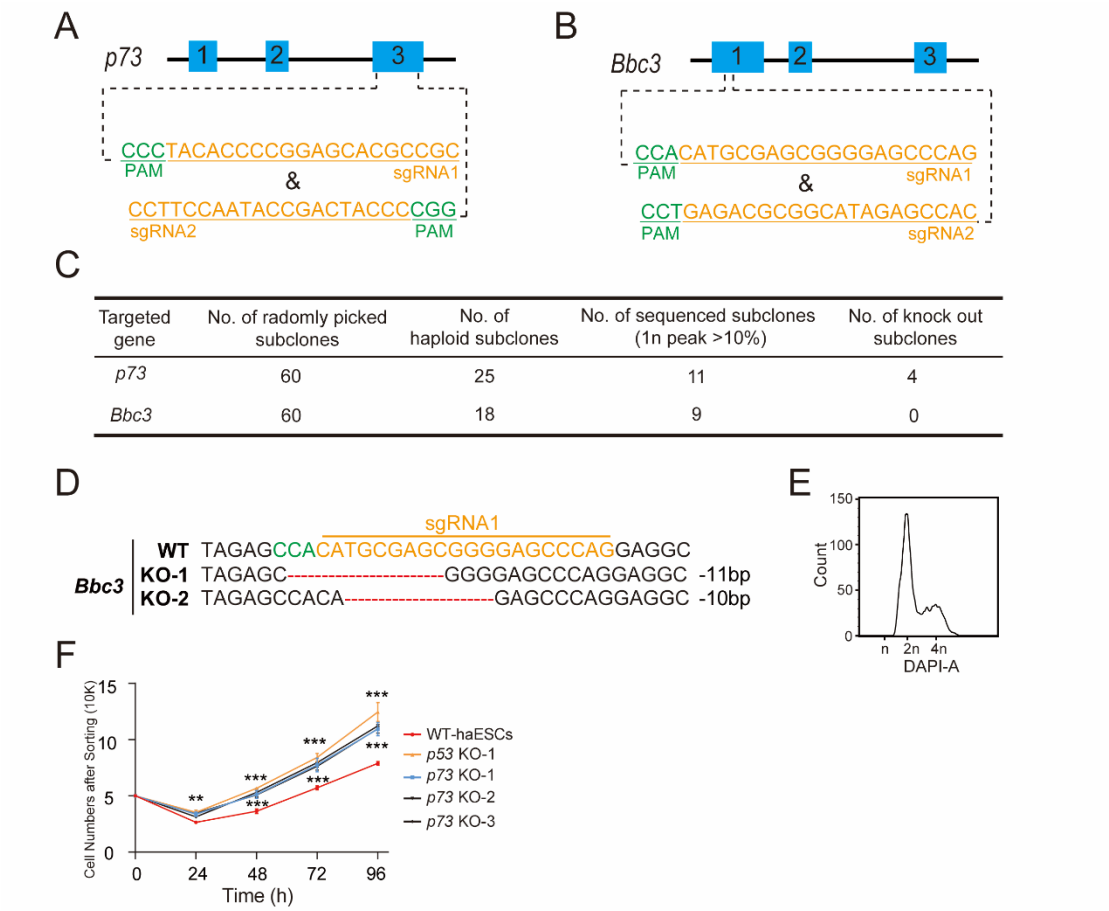

Targeted gene	No. of radomly picked subclones	No. of haploid subclones	No. of sequenced subclones (1n peak >10%)	No. of knock out subclones
p73	60	25	11	4
Bbc3	60	18	9	0

Figure S5. Gene function validation of *p73* and *Bbc3* in haESCS. Related to Figure 5

(A-B) DNA information for knocking out of *p73* and *Bbc3* in WT-haESCs using the CRISPR/Cas9 system.

(C) Summary of haploidy and gene mutations in *p73*-KO and *Bbc3*-KO ESCs. 25/60 subclones of *p73*-KO and 18/60 subclones of *Bbc3*-KO were haploid. The subclones whose 1n peak >10% were sequenced, and there were 4 *p73*-KO subclones but no *Bbc3*-KO subclone.

(D) *Bbc3*-KO genotypes in the mixture *Bbc3*-KO ESCs.

(E) DNA content analysis of *Bbc3*-KO ESCs. The percentage of the 1n peak (G0/G1 phase) was 0%.

(F) Cell counts of *p53* KO-1, *p73* KO-1, *p73* KO-2 and *p73* KO-3 for 24 h, 48 h, 72 h and 96 h after sorting, with WT-haESCs as a control. (n=3 independent experiments). t test, **p < 0.01, ***p < 0.001. Data are represented as the mean ± SEM.

Table S1. Contribution of *p53*-KO ESCs in chimeric embryos. **Related to Figure 3.**

	Percentage of GFP+ cells (%)[a]		Percentage of cells in the 1n peak (%)[b]
	p53-KO haploid	*p53*-KO diploid	*p53*-KO haploid
E6.5	17.2	ND[c]	28.5
	55.5	ND	24.5
E8.5	12.4	24.9	25.3
	37.6	40.3	24.3
E10.5	1.6	ND	21.4
	3.3	ND	22.3

[a]The percentage of GFP+ cells were calculated based on all cells dissected from respective chimeric embryo by FACS analysis.

[b]The percentage of cells in the 1n peak were calculated based on GFP+ cells from respective chimeric embryo by FACS analysis.

[c]ND, not determined.

Table S4. Summary of used primers. Related to Experimental Procedures and Figures 1-5, S1 and S5

Type	Target Name	Sequence 5'-3'
***p53* knockout sgRNA**	sgRNA1-1	CACCGAGGAGCTCCTGACACTCGGA
	sgRNA1-2	AAACTCCGAGTGTCAGGAGCTCCTC
	sgRNA2-1	CACCGACCCTGTCACCGAGACCCCT
	sgRNA2-2	AAACAGGGGTCTCGGTGACAGGGTC
***Bbc3* knockout sgRNA**	sgRNA1-1	CACCGGTGGCTCTATGCCGCGTCTC
	sgRNA1-2	AAACGAGACGCGGCATAGAGCCACC
	sgRNA2-1	CACCGCTGGGCTCCCCGCTCGCATG
	sgRNA2-2	AAACCATGCGAGCGGGGAGCCCAGC
***p73* knockout sgRNA**	sgRNA1-1	CACCGCCTTCCAATACCGACTACCC
	sgRNA1-2	AAACGGGTAGTCGGTATTGGAAGGC
	sgRNA2-1	CACCGGCGGCGTGCTCCGGGGTGTA
	sgRNA2-2	AAACTACACCCCGGAGCACGCCGCC
***p53* overexpression**	*p53*	F: GCTCTAGAATGACTGCCATGGAGGAGTC
	p53	R: CGGAATTCTCAGTCTGAGTCAGGCCCCA
***Cdk2* overexpression**	*Cdk2*	F: GCTCTAGAATGTCGGGTCCGCGCGCG
	Cdk2	R: CGGAATTCTCACTGCTCAATTTCATGGGTGCCAG
***MAPK11* overexpression**	*MAPK11*	F: CGTACCGGTATGGAGAACTTCCAAAAGGTGGA
	MAPK11	R: CGGAATTCTCAGAGCCGAAGGTGGGGC
qPCR	*Gapdh*	F: AGGTCGGTGTGAACGGATTTG
	Gapdh	R: TGTAGACCATGTAGTTGAGGTCA
	Oct4	F: GGATGGCATACTGTGGACCTC
	Oct4	R: TTTCATGTCCTGGGACTCCTCG
	Nanog	F: CCAGGGCTATCTGGTGAACG
	Nanog	R: CCCGAAGTTATGGAGCGGAG
	p53	F: CATGAACCGCCGACCTATCC
	p53	R: GCAGTTCAGGGCAAAGGACT
	p21	F: CCCGAGAACGGTGGAACTTT
	p21	R: AGAGTGCAAGACAGCGACAA
	Cyclin B	F: GACGCAGATAGTGGGGCTG
	Cyclin B	R: GCAATAAACATGGCCGTTACACC
	Cdk2	F: CCTGCTTATCAATGCAGAGGG
	Cdk2	R: TGCGGGTCACCATTTCAGC
	Rex1	F: CCCTCGACAGACTGACCCTAA
	Rex1	R: TCGGGGCTAATCTCACTTTCAT
	Hand1	F: GGCAGCTACGCACATCATCA
	Hand1	R: GCATCGGGACCATAGGCAG
	Cdx2	F: GTCCCTAGGAAGCCAAGTGAA
	Cdx2	R: TTGGCTCTGCGGTTCTGAAA
	FGF5	F: GAAGCGTCTCACTCCCGAAG
	FGF5	R: GAAGAAAACGTCGCGCTACT

	Nestin	F: CCCTGAAGTCGAGGAGCTG
	Nestin	R: CTGCTGCACCTCTAAGCGA
	T	F: GCTTCAAGGAGCTAACTAACGAG
	T	R: CGTCACGAAGTCCAGCAAGA
	Klf4	F: TCGCAGTCATGTGTGTGCTC
	Klf4	R: GCCTCCGGTCCTTCACTAGG
	Otx2	F: ACACACGAGGTAGTGACGC
	Otx2	R: TCTGAGTCGCCGTGGAAAAG
	p73	F: ATGCTTTACGTCGGTGACCC
	p73	R: GCACTGCTGAGCAAATTGAAC
	MAPK11	F: GCGGGATTCTACCGGCAAG
	MAPK11	R: GAGCAGACTGAGCCGTAGG
	Phlda3	F: CCGTGGAGTGCGTAGAGAG
	Phlda3	R: TCTGGATGGCCTGTTGATTCT
	Bbc3	F: AGCAGCACTTAGAGTCGCC
	Bbc3	R: CCTGGGTAAGGGGAGGAGT
	Bax	F: TGAAGACAGGGGCCTTTTTG
	Bax	R: AATTCGCCGGAGACACTCG

Supplemental Experimental Procedures

Mice

All the specific pathogen-free (SPF)-grade mice were purchased from Beijing Vital River Laboratory Animal Technology Co., Ltd. and housed at the Nankai University Animal Center. All experiments were guided by the Institutional Animal Care and Use Committee of Nankai University, and all experiments conformed to the relevant regulatory standards.

Cell Culture

HaESCs were derived from chemically activated oocytes with a 129Sv/Jae genetic background as described previously (Gao et al., 2018). The culture medium of the haESCs referred to a previous protocol (Shuai et al., 2014). For the purification of haploids, haESCs were incubated with 5 μg/ml Hoechst 33342 (Invitrogen, H3570) for 20 min at 37℃. Subsequently, the haploid (1n) peak was gated to sort cells with a diploid control on a Moflo XDP sorter (Beckman). For DNA content analysis, cell samples were fixed with 75% ethanol overnight and then incubated with 50 μg/ml propidium iodide (Sigma, P4170) for 30 min at 37℃. Subsequently, the haploid (1n) peak was analyzed with a diploid control on a BD LSR Fortessa flow cytometer.

Vector Construction

For the *p53*-, *Bbc3*- or *p73*- knockout vector, sgRNAs were designed with reference to the CRISPR design tool (www.crispr.mit.edu), then annealed and inserted into SpCas9n (BB)-2A-GFP (PX461, Addgene, #48140) vectors. For the *p53-, Cdk2*- and *MAPK11*- overexpression vector, the cDNA of *p53, Cdk2* and *MAPK11* were amplified from the total cDNA of mouse ESCs by using Phanta Max Super-Fidelity DNA Polymerase (Vazyme, P505-d2). Then, *p53, Cdk2* and *MAPK11* cDNA was linked in the reconstructive *PiggyBac* Dual promoter (SBI, PB513B-1) separately by using the BamHI and EcoRI sites (*p53*), AgeI and EcoRI sites (*Cdk2*) and XbaI and EcoRI sites (*MAPK11*). All the primers used are listed in Table S2.

Quantitative Real-time PCR

Following the manufacturer's protocol to purify total RNAs from cells using TRIzol Reagent (Invitrogen, 15596018), cDNA was obtained by reverse transcription using a Prime Script™ RT reagent Kit with a gDNA Eraser (Takara, RR047A). Quantitative real-time PCR was performed on an ABI QuantStudio™ 6 Flex machine with FS Universal SYBR Green Master (Roche, 4913914001). Relative expression levels were normalized to *Gapdh*. Averages and SD values were calculated based on three independent experiments. All primers used are listed in Table S2.

Western Blotting

For western blotting experiments, protein samples were extracted from cells by using RIPA lysis solution (Solarbio, R0020) following the manufacturer's protocol. Equal amounts of the samples were separated by SDS-PAGE and transferred to a polyvinylidene fluoride (PVDF) membrane (GE, RPN303F). The membranes were blocked in 5% nonfat dry milk for 2 hours, washed three times with PBST, and incubated with primary antibodies overnight at 4°C. Then, the membranes were washed and incubated with appropriate secondary antibodies for 1 hour at room temperature. The signal was detected with Enlight™ (Engreen, 29050) and imaged. The primary antibodies used in western blotting included anti-P53 (Santa, sc-126), anti-P73 (Abcam, ab40658) and anti-GAPDH (Santa, sc-365062).

T7ENI Assay

Following the manufacturer's recommended protocol for T7 Endonuclease I (NEB, E3321), the DNA fragments containing sgRNA target sites were amplified from transfected cells and wild-type cell genomic DNA by using Phanta Max Super-Fidelity DNA Polymerase (Vazyme). These two kinds of

DNA fragments were hybridized in Buffer 2.0 (NEB). After the hybridization reaction, T7 Endonuclease I was added to the mixture, and digestion was performed for 2 hours at 37 °C. The products were analyzed by agarose gel electrophoresis.

Immunostaining, AP staining, and Karyotype Analysis

For immunofluorescence analysis, cells were fixed with 4% paraformaldehyde at 4°C overnight. The samples were washed three times with PBS. Then, the cells were permeabilized with 0.3% Triton X-100 (Sigma, T9284) for 40 minutes and incubated with 1% BSA (Sigma, B2064) for 40 minutes at room temperature. Next, the samples were incubated with primary antibodies against OCT4 (Abcam, ab18976), SSEA1 (Santa, sc-21702), NANOG (Abcam, ab80892), TFE3 (Sigma, HPA023881), PAX6 (Abcam, ab5790), SOX1 (Abcam, ab87775), NESTIN (Abcam, ab6320), O4 (R&D Systems, MAB1326), NEUN (Abcam, ab104225), GFAP (Abcam, ab7260), MAP2 (Abcam, ab32454) and TUJ1 (Abcam, ab18207) at 4°C overnight. The primary antibodies were diluted in blocking buffer (1% BSA). After three wash steps, the cells were stained with secondary antibodies at room temperature for 1 hour. After another three wash steps, the nuclei were stained with DAPI (YEASEN, 40727ES10) for 10 minutes at room temperature. Immunofluorescence images were taken with a TCS SP8 confocal laser scanning microscope (Leica). AP staining was performed according to the manufacturer's instructions for the alkaline phosphatase kit (Beyotime, P0321). For karyotype analysis, cells were incubated with 0.2 μg/mL nocodazole (MCE, HY-13520) overnight. The samples treated with hypotonic solution were fixed in methanol: acetic acid (3:1) for 20 min twice and dropped onto precooled slides. Then, the cells were stained with Giemsa for 15 min before observation.

Analysis of RNA-seq Data

All the RNA-seq data were sequenced by a local company (Novogene). For data analysis, quality control was performed for the raw sequencing reads using the FastQC application. Raw data were trimmed using Trimmomatic to remove low-quality bases (quality score < 5) or reads (low-quality bases > 50% of the read size)(Bolger et al., 2014). Then, the abundance of each transcript was quantified using Salmon (Patro et al., 2017). Differential gene expression analysis was performed using the DEseq2 package, and gene expression was normalized using the relative-log-expression (RLE) in DESeq2 (Love et al., 2014). Genes with summed reads greater than 10 across all samples were kept. The R function of heatmap was used to generate the hierarchical clustering of the top 50 variant genes. Scatterplots were visualized with ggplot2 and ggrepel.

For Gene Ontology analysis, metascape (http://metascape.org) was employed to perform gene enrichment and functional annotation analyses in both WT ESCs and *p53* KO-1 cells with the following ontology sources: KEGG Pathway, GO Biological Processes, and Reactome Gene Sets(Zhou et al., 2019). Genes with p-values < 0.001, a minimum count of 3, and an enrichment factor > 1.5 were identified and grouped into clusters based on their membership similarities.

Cell Survival Test, Cell Growth Curve and Caspase-3 Activity

For the cell survival test, 50,000 haploid cells were sorted and plated in a 24-well plate under feeder-free conditions. Each group included three repetitions. After 24 hours, the cells were digested into single cells and counted with a cell counter (Logos Biosystems, LUNAII). To describe the cell growth curve, the number of living cells was recorded at 24, 48, 72 and 96 hours. Averages and SD values were calculated based on three independent experiments.

To analyze the rate of diploidization, purified *p53*-KO, *p73*-KO and WT-haESCs were passaged every 2-3 days. Then, the haploid proportions were analyzed at 10 days, 14 days, 28 days and 35 days after sorting and calculated according to a previous report (Xu et al., 2017). Averages and SD values were

calculated based on three independent experiments. For the Caspase-3 activity, 5×10^5 haploid cells were sorted and plated in a 35 mm petri-dish under feeder-free condition. After 24 hours, the Caspase-3 activity was detected by the Caspase 3 Activity Assay Kit (Beyotime, C1116) follow the instructions. Averages and SD values were calculated based on three independent experiments.

Supplemental References

Bolger, A.M., Lohse, M., and Usadel, B. (2014). Trimmomatic: a flexible trimmer for Illumina sequence data. Bioinformatics *30*, 2114-2120.

Gao, Q., Zhang, W., Ma, L., Li, X., Wang, H., Li, Y., Freimann, R., Yu, Y., Shuai, L., and Wutz, A. (2018). Derivation of Haploid Neural Stem Cell Lines by Selection for a Pax6-GFP Reporter. Stem cells and development *27*, 479-487.

Love, M.I., Huber, W., and Anders, S. (2014). Moderated estimation of fold change and dispersion for RNA-seq data with DESeq2. Genome biology *15*, 550.

Patro, R., Duggal, G., Love, M.I., Irizarry, R.A., and Kingsford, C. (2017). Salmon provides fast and bias-aware quantification of transcript expression. Nature methods *14*, 417-419.

Shuai, L., Li, W., Wan, H., Zhao, X.Y., Wang, L., and Zhou, Q. (2014). Generation of Mammalian offspring by haploid embryonic stem cells microinjection. Current protocols in stem cell biology *31*, 1A 6 1-15.

Xu, H., Yue, C., Zhang, T., Li, Y., Guo, A., Liao, J., Pei, G., Li, J., and Jing, N. (2017). Derivation of Haploid Neurons from Mouse Androgenetic Haploid Embryonic Stem Cells. Neuroscience bulletin *33*, 361-364.

Zhou, Y., Zhou, B., Pache, L., Chang, M., Khodabakhshi, A.H., Tanaseichuk, O., Benner, C., and Chanda, S.K. (2019). Metascape provides a biologist-oriented resource for the analysis of systems-level datasets. Nature communications *10*, 1523.